Open Access

Research Article

PRNANO

Precis. Nanomed. 2019;2(4):393-439

ANDOVER HOUSE

Protein Binding Effects of Dopamine Coated Titanium Dioxide Shell Nanoparticles

Ruben Omar Lastra[a], Tatjana Paunesku[a], Barite Gutama[a], Filiberto Reyes, Jr.[a], Josie François[a], Shelby Martinez[a], Lun Xin[a], Koshonna Brown[a], , Alia Zander[a], Sumita Raha[a], Miroslava Protic[a], Dhaval Nanavati[b], Yingtao Bi[c], Gayle E Woloschak[a#]

[a] *Department of Radiation Oncology Feinberg School of Medicine, Northwestern University, Chicago, Illinois 60611, United States*

[b] *Chemistry of Life Processes Institute, Proteomics Core, Northwestern University, Evanston, Illinois 60208, United States*

[c] *Department of Biomedical Informatics, Feinberg School of Medicine, Northwestern University, Chicago, Illinois 60611, United States*

Submitted: August 2, 2019 Accepted: September 17, 2019 Published: October 2, 2019

Graphical Abstract

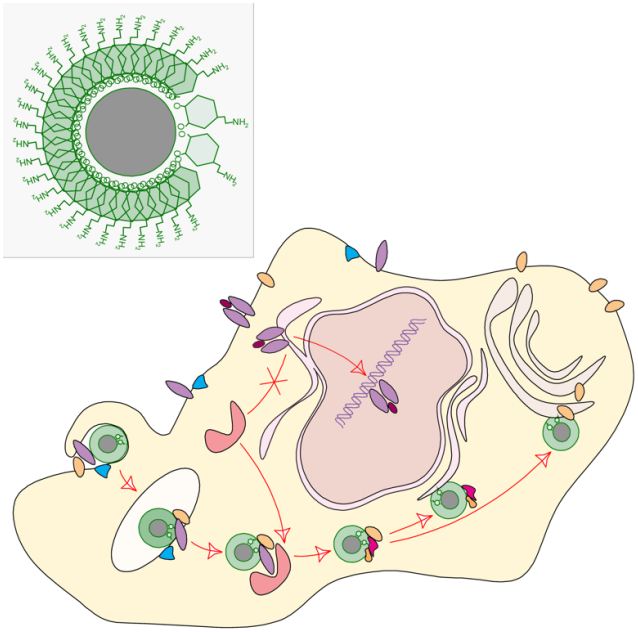

Metal oxide nanoparticles covered with dopamine (inset) enter cancer cells non-specifically (e.g. micropinocytosis), traverse intracellular vesicles and cytosol and interact with numerous proteins that change over time.

Abstract

Non-targeted nanoparticles are capable of entering cells, passing through different subcellular compartments and accumulating on their surface a protein corona that changes over time. In this study, we used metal oxide nanoparticles with iron-oxide core covered with titanium dioxide shell (Fe_3O_4@TiO_2), with a single layer of covalently bound dopamine covering the nanoparticle surface. Mixing nanoparticles with cellular protein isolates showed that these nanoparticles can form complexes with numerous cellular proteins. The addition of non-toxic quantities of nanoparticles to HeLa cell culture resulted in their non-specific uptake and accumulation of protein corona on nanoparticle surface. TfRC, Hsp90 and PARP were followed as representative protein components of nanoparticle corona; each protein bound to nanoparticles with different affinity. The presence of nanoparticles in cells also mildly modulated gene expression on the level of mRNA. In conclusion, cells exposed to non-targeted nanoparticles show subtle but numerous changes that are consistent from one experiment to another.

To whom correspondence should be addressed. Email: g-woloschak@northwestern.edu

Keywords:

Nanoparticles, Protein Corona, Cellular Pathways

Purpose and Rationale

Non-targeted nanoparticles are often taken up by cells non-specifically through all possible endocytic mechanisms. As they enter cells, reside in endosomes or get released into different subcellular compartments, nanoparticles encounter numerous proteins, interacting with them and their protein partners creating complexes of variable permanence and stability. Purpose of this study was to explore some of these interactions using dopamine coated Fe_3O_4@TiO_2 nanoparticles and document their effects on cells.

Introduction

Prediction of nanoparticle behavior is difficult even with the best characterized nanomaterials and experimental systems [1]. One of the well-known, yet insufficiently understood reasons for this is that nanoparticles adsorb proteins in extracellular and intracellular milieus. These protein layers are referred to as the "protein corona" and an increasing body of literature emphasizes the importance of the protein corona for the subsequent fate of nanoparticles and their effects on cells and organisms [2, 3]. Research interest in nanoparticle protein coronas and their components is often focused on potential modification(s) of nanoparticle trafficking and function [4, 5]. Studies exploring cellular responses to nanoparticles accumulating surface proteins, on the other hand, emphasize modulations of cellular processes such as changes of focal adhesion points[6] and cytoskeleton rearrangements [7], etc.

In the past, we have investigated interactions between nanoparticles and biological molecules, cells and subcellular compartments, dividing our attention between targeted [8-15] and non-targeted [16-19] nano-constructs prepared as iron oxide, titanium oxide or the combinations of these two materials. Others have also worked with different versions of titanium dioxide (TiO_2) based nanoparticles both in vitro and in vivo, focusing on primary and cancer cell lines and organisms such as drosophila, zebrafish, mutant and wild-type mice etc. [8-26]. The majority of these cell culture studies used nanoparticle concentrations in the toxic range, above 25 micrograms of TiO_2 per mL depending on the biological system, size and crystalline form of TiO_2 and other experimental conditions [25, 27].

In this work we use a non-targeted nano-construct – dopamine covered nanoparticles with an iron-oxide core and a titanium dioxide shell (Fe_3O_4@TiO_2) and investigate interactions of this nanomaterial with the intracellular milieu of HeLa cells. The concentration of nanoparticles used (20 μg/mL of TiO_2) is below cytotoxic levels and the period of nanoparticle incubation with cells in this study lasted as long as 24 hours with intermittent cell harvest for mRNA and protein isolation. Our interest was to evaluate protein corona of nanoparticles present in cells whose viability was not compromised – a situation similar to one that can be expected when exposure to nanoparticles is relatively low and not a part of a clinical treatment, for example. In our previous work we have explored nanoparticles functionalized by different targeting molecules [8-10, 14, 15, 28] attached via dopamine or dopac. While uptake of these nano-constructs was targeted and nanoparticles made to be toxic such as due to white light activation and DNA cleavage [8, 9]; nanoparticles that failed functionalization with targeting moieties and carrying dopamine alone could be expected to enter any cell by non-specific endocytosis as we have shown in the past [19].

Methods

Nanoparticle Preparation:

All chemicals for the preparation of nanoparticles were purchased from Sigma (Sigma-Aldrich Corp., St. Louis, MO). Nanoparticles were synthesized as described before [8, 9, 17, 28] with TiO_2 shell deposition by hydrolysis of $TiCl_4$ under conditions that favor production of ultrasmall anatase TiO_2 nanoparticles [29-31]. Synthesis of TiO_2 shell was done in an ice cooled bath by adding $TiCl_4$ chilled to -20°C dropwise to a diluted colloidal suspension of Fe_3O_4 nanoparticles. Synthesis of iron oxide nanoparticles was described elsewhere [8, 9, 17, 28]; briefly, a combination of $FeCl_2$ and $FeCl_3$ in 24 mM citric acid was steered for 3 hr at room temperature and aged in static air at 70°C

for 24 hours, forming the Fe_3O_4 core nanoparticles 1.5 to 3 nm in size. These particles were covered with a TiO_2 shell layer, for a final nanoparticle size between 10-20 nm (Supplemental Figure 1). In the course of the synthesis a color change of nanoparticle suspension was noted from rust (pure iron oxide nanoparticle solution) to pale yellow (core-shell nanoparticle solution). Nanoparticle sizing was done by cryo transmission electron microscopy on a JEOL 1230 120 kV Transmission Electron Microscope at the Northwestern University Biological Imaging Facility (BIF) (Supplemental Figure 1). Final TiO_2 concentration in colloidal nanoparticle suspension was 200 µg/mL as measured at the Northwestern University Quantitative Bio-element Imaging Center (QBIC) using an X Series II Inductively Coupled Plasma-Mass Spectrometer (Thermo Fisher Scientific, West Palm Beach, FL). A series of standards ranging from 0 ppb to 50 ppb titanium was used. All standards and samples were spiked with 3 ppb of indium as an internal control. Using the approach explained before [8, 9, 17] we calculated that this corresponds to an approximate 180 nM nanoparticle concentration (for a nanoparticle size of 10 nm), with an approximate 300 µM concentration of surface binding sites. The complete TiO_2 shell surface was covered with dopamine by dissolving 21 mg of powdered dopamine in 55 mL of as-prepared nanoparticle colloid (pH~1). The final concentration of dopamine was 2mM, several fold greater than the molarity of available nanoparticle surface sites. The newly coated nanoparticles were dialyzed in 10 mM sodium phosphate and 40 mM sodium chloride buffer pH~4.5 in order to stabilize the covalent bond between dopamine and TiO_2 surface and remove excess dopamine. Use of dialysis tubing (Slide-A-Lyzer™ Dialysis Cassettes, Thermo Fisher Scientific, West Palm Beach, FL) with 2 KDal pores allowed removal of unbound dopamine from the nanoparticle mixture. If any of the TiO_2 molecules on nanoparticle surface were free at the time of dialysis, they could have bound to phosphates through hydrogen bonds [32]; more importantly, dialysis provided chloride and phosphate ions that could neutralize NH_3^+ group of dopamine and change polarity of nanoparticles. In the course of dialysis nanoparticle colloidal mixture changed appearance from a transparent pale yellow liquid to a partially opaque light brown solution. This red shift in nanoparticle absorption is characteristic for covalently modified TiO_2 nanoparticle surface [31] (Supplemental Figure 2). Nanoparticles remained stable in solution for more than 6 months. Nanoparticles were further diluted in 10mM sodium chloride and evaluated by Zetasizer Nano (Malvern, Worcestershire, United Kingdom); zeta potential of dopamine-coated and dialyzed nanoparticles was -27mV and their hydrodynamic diameter about 90nm, with the formation of aggregates with a hydrodynamic diameter of about 900 nm (Supplemental Figure 3). This work was performed at the Northwestern University's Analytical BioNanoTechnology Equipment Core of the Simpson Querrey Institute.

Cell Culture and Nanoparticle Treatments:

Cervical cancer cell line HeLa (CCL-2 ATCC, Manassas, Virginia) was grown in DMEM supplemented with 10% fetal bovine serum and 1% penicillin/streptomycin (all obtained from Corning Cellgro, Fisher Scientific) at 37 °C and 5% CO_2. Intermittent mycoplasma testing consisted of optical fluorescence imaging of cells grown on microscope slides and stained with in phosphate buffered saline (PBS) with 0.01mg/mL of 4',6-Diamidino-2-Phenylindole, Dihydrochloride (DAPI) (Sigma-Aldrich Corp., St. Louis, MO), similar to work of others [33].

Cells were counted before plating using a Bio-Rad TC20 (Bio-Rad, Hercules, CA) automated cell counter. Either 5×10^5 or 10^6 cells were plated per T25 flask 16-18h prior to treatment; these cell densities corresponded roughly to 40% and 80% confluent cells monolayers 16-18 hours later when nanoparticle treatments had begun.

Dialyzed dopamine coated nanoparticles were added as 1/10th of the volume to 5 mL of complete media per T25 flask. The final concentration of TiO_2 in media was 20 µg/mL (or, in standard T25 flasks, 4 µg/cm2). Each nanoparticle-exposed cell flask was paired with an untreated control flask in all protein and mRNA isolations and assays.

Staurosporine treatment:

HeLa cells were seeded to achieve 40% confluence in 16-18 hours. Dopamine covered

Fe_3O_4@TiO_2 nanoparticles were given to selected flasks of cells for 2 hours followed by treatment with staurosporine (1 µM, 0.1 µM or 0.01 µM) for 4 hours. Staurosporine (Enzo Scientific, Farmingdale, NY) was dissolved in dimethyl sulfoxide (DMSO) at 1mM concentration. DMSO alone served as a negative control.

Protein Extracts:

HeLa cells were plated in T-25 flasks at densities of 5×10^5 or 1×10^6 at 16 hours before the beginning of the experiment. The cells were then washed three times with PBS and resuspended in 100 µL of RIPA buffer (Thermo Scientific 89900) with Protease inhibitors (diluted from 1x to 100x) (Calbiochem 539131). Each flask was scraped and the liquid (mixture of cells and buffer) was removed from the flask and transferred to a new microcentrifuge tube. Samples were then rocked at medium speed in 4 °C for 15 minutes. Next, the tubes were centrifuged in 4 °C for 15 min at maximum speed, the supernatant was transferred to a new microfuge tube and the protein concentration was calculated using Bradford reagent (Bio-Rad 5000-0205) and the NanoDrop-3000 (NanoDrop, Wilmington, DE) and BSA (2000 µg/mL) (Bio-Rad 500-0206) was used as a standard.

Isolation and Partial Characterization of Proteins Adhering to Nanoparticles:

HeLa cell nuclear and cytoplasmic lysates were prepared using standard procedures. In short, cells washed in PBS were resuspended in 5 V (compared to cell V) of buffer A (10 mM Tris 10 mM KCl, 1.5 $MgCl_2$, pH~7.9, 0.5 mM DTT), spun for 5 minutes at 3000 rpm, resuspended in 2 V of buffer A for 10 minutes on ice and broken into cytosolic fraction and nuclei by homogenization. Nuclei were resuspended in 0.5 V buffer C (20 mM Tris pH7.9, 0.02 M KCl, 1.5 mM $MgCl_2$, 25% glycerol, 0.5 mM DTT and 0.2 mM PMSF) and mixed gently with equal V of buffer D (20 mM Tris pH7.9, 1.2 M KCl, 1.5 mM $MgCl_2$, 25% glycerol, 0.5 mM DTT and 0.2 mM PMSF) and steered for 30 minutes. Both fractions were centrifuged at 13,000 g in in a tabletop centrifuge (Beckman-Coulter, Indianapolis, IN) for 30 minutes before incubation of supernatant with nanoparticles. Protein extracts (200 µg of each) were incubated with 100 µL nanoparticles for 16 hours on a rocking platform at 4 °C. Protein and nanoparticle pellets were "washed" by resuspending-centrifugation in 2x Laemmli Sample Buffer three times. Finally, beta-mercaptoethanol (Sigma-Aldrich, St Louis, MO) was added to the mixtures and they were heated at 95 °C for 5 minutes to denature and separate the more resistant protein corona from the nanoparticles. Samples were briefly spun to remove residual nanoparticles and the supernatants were loaded onto gradient (4-20%) SDS-PAGE gels. Gels were run and stained with Comassie Blue (Bio-Rad, Hercules, CA). Nuclear and cytoplasmic extracts (Supplemental Figure 4) were loaded on the gel as controls. Areas with protein bands enriched in lanes where proteins were stripped from nanoparticles were selected for further work. Pieces of gel containing multiple bands of proteins were excised and submitted for processing to the NU Protein core facility. Briefly, protein was digested with 200 ng of sequencing grade trypsin (Sigma-Aldrich Corp., St. Louis, MO) at 37°C for 18 hr. The digested protein preparation was dried, resuspended in 500 µL of 5% acetonitrile, 0.1% formic acid (Sigma-Aldrich Corp., St. Louis, MO) and desalted using C18 spin columns (Thermo Fisher Scientific, West Palm Beach, FL). The desalted peptides were loaded onto a 10 cm long, 75 µM reversed phase capillary column (ProteoPep™ II C18, 300 Å, 5 µm size, New Objective, Woburn, MA) and separated with a 100 min gradient from 5% acetonitrile to 100% acetonitrile on a Proxeon Easy n-LC II (Thermo Fisher Scientific, West Palm Beach, FL). The peptides were directly eluted into an LTQ Orbitrap Velos mass spectrometer (Thermo Fisher Scientific, Waltham, MA USA) with electrospray ionization at 350 nL/min flow rate. The peptide MS data were analyzed using Proteome Discoverer (version 1.3, Thermo Fisher Scientific) and searched using an in-house MASCOT server against the Swiss-Prot database (version 2011_12). The species filters for database search for samples was Homo sapiens.

Protein Isolation from Nanoparticle Treated Cells and Isolation of Proteins Adhering to Nanoparticles:

After nanoparticle treatments of 0, 1, 2, 4, 6 or 24 hours, nanoparticle treated and control cells were washed three times with PBS (Thermo Fisher Scientific, West Palm Beach, FL) and collected in 100 µL of RIPA buffer (Thermo Fisher Scientific, West Palm Beach,

FL) with Protease inhibitors (Calbiochem). Cells were collected by scraping and rocked at 4 °C for 15 minutes. According to the standard procedure, cell lysates were centrifuged at 13,000 g for 15 minutes at 4°C in a tabletop centrifuge (Beckman-Coulter, Indianapolis, IN) to separate proteins from cell debris and the supernatant was transferred to a new microfuge tube. The protein concentration was calculated using Bradford assay with BSA as a standard using NanoDrop 2000 (Thermo Fisher Scientific, Waltham, MA USA); all Bradford assay chemicals came from Bio-Rad (Hercules, CA).

For isolation of proteins forming corona on nanoparticles initial steps for protein isolation were done as above. After cell lysis however, the supernatant was removed and the pellet resuspended in 200µL 2X Laemmli Sample Buffer (Bio-Rad, Hercules, CA). The resuspended pellet was then centrifuged for 10 min at 10,000g, the supernatant was removed and saved ("the first wash") and this was repeated two more times ("second and third washes"). Finally, the pellet was resuspended in 80 µL of Laemmli Sample Buffer, boiled at 95 °C for 10 minutes, spun to remove the residual nanoparticle aggregates and loaded on a gel.

Western Blots:

Immunoblots were done with protein extracts adjusted to same concentration by diluting with PBS and mixing 1:1 with 4X Laemmli Sample Buffer (Bio-Rad 161-0747). Samples were then separated with a Bio-Rad gradient SDS Gel (4-20%) (Bio-Rad 456-8093). Afterwards, the samples were transferred to a nitrocellulose membrane (Bio-Rad 162-0145) that was blocked by 5% skimmed milk (Bio-Rad 170-6404) in 1× TBS-T (Tris-NaCl-Tween 20) for 2 hours and then incubated overnight with primary antibodies: Hsp90 (Ab13495 1:10,000), , PARP (Ab32138, 1:5:000), and Apoptosis Western Blot Cocktail (pro/p17-caspase 3, cleaved-PARP, muscle actin) (ab136812, 1:250). The membrane was washed three times with 1× TBS-T and then probed with secondary antibodies (1:10,000) (Cell Signaling 7074S and 7076S) tagged with horseradish peroxidase (HRP) and incubated for 1 h at room temperature. The membrane was overlaid with Clarity Western ECL Substrate (Bio-Rad 1705061) according to the manufacturer's instructions, and the blots were developed.

RNA Isolation:

HeLa cells were plated and treated with nanoparticles as above; harvest was done at 2h and 4h timepoints. Total RNA was isolated using the PureLink RNA Mini kit (12183020 Thermo Fisher Scientific, West Palm Beach, FL). RNA quantity was assessed with a NanoDrop 2000 Spectrophotometer (Thermo Fisher Scientific, Wilmington, Delaware).

RNA was submitted to NU Center for Genetic Medicine core facility for processing. RNA quality evaluation was done using Agilent 2100 bioanalyzer (Agilent, Santa Clara, CA); RIN of ten was obtained for all samples and HumanHT12-v4 Illumina arrays (Illumina Inc., San Diego, CA) were used for gene expression evaluation. Four sets of biological replicates were prepared and tested, as well as one technical replicate. All of the samples met the Illumina quality checks. Initial data quality checks were performed using Bioconductor Lumi package [39]. Raw array data was submitted to Gene Expression Omnibus (GEO) database (www.ncbi.nlm.nih.gov/geo/) under accession number GSE88786. Subsequent analysis included ComBat [40] analysis in order to remove batch effects; final data output was obtained using Limma model [41] with cutoff q-value = 0.1.

Quantitative Real-time Polymerase Chain Reaction (QRT-PCR):

For each sample 1 µg of total RNA was reverse transcribed using the High-Capacity RNA-to-cDNA™ Kit (4387406 Thermo Fisher Scientific, West Palm Beach, FL).PCR was done using Power SYBR Green PCR Master Mix (4367659 Thermo Fisher Scientific, West Palm Beach, FL) and 250 nM of specific primers in a total volume of 25 µL in a 7300 Real Time PCR system (Applied Biosystems, Foster City, CA) Samples were tested at least in triplicate and up to six times on the same plate (samples values closest to the mean were used for analysis) and negative control PCR amplification, with water instead of cDNA, was performed for every plate and every primer pair. After incubation for two minutes at 50 °C and a denaturation step of 10 minutes at 95 °C, samples were subjected to 40 cycles (30 seconds at 95 °C, 30 seconds at 60 °C, 30 seconds at 72 °C), following by the acquisition of the melting curve. One reference gene was used: beta-actin. Predesigned primers were

purchased from Integrated DNA Technologies, Inc. (IDT, Coralville, Iowa). Primer pairs specific for transferrin receptor: Hs.PT.58.22906586, Hsp90: Hs.PT.58.38593314.g; GPER: Hs.PT.58.1412417; MAP3K14: Hs.PT.58.14658535; ID1: Hs.PT.58.18791272.g; ID2: Hs.PT.58.38958353; ID3: Hs.PT.58.27440053.g; Dusp2: Hs.PT.58.39972211.g; CLDN15: Hs.PT.58.20001672; SMUG: Hs.PT.58.27762894; FZD9: Hs.PT.58.4929232.g were obtained. Primer pair for PARP1 was obtained from Sigma (Sigma-Aldrich Corp., St. Louis, MO); it included sense 5'CTTGGACCGAGTAGCTGATGG (positions 1008 to 1028 in reference sequence NM_001618.3) and antisense (pos. 1100 to 1120 5'AGTGCAGTAATAGGCATCGCT primers.

Ct for each one of the three biological replicate PCR reactions (each with >= 3 technical replicates) was calculated from technical replicates; these were selected to fulfill the criteria for low variance (less than 0.5 Ct values from each other) and averaged. Standard deviation for average ΔΔCt values from three biological replicates was calculated for each mRNA and timepoint. Statistical significance was calculated by doing an f-test and determining if the samples had similar variance or not, followed by the appropriate t-test (two-sample assuming equal variances or two-sample assuming unequal variances) to determine statistical significance.

Bioinformatics analysis:

Pathway analysis for gene IDs for proteins attached to nanoparticles as well as mRNAs was done using DAVID Bioinformatics Resources https://david.ncifcrf.gov/home.jsp sponsored by the NIAID, NIH [31, 32].

Results

Nanoparticles of the final size between 10-20 nm were made from 2 nm Fe_3O_4 cores overlaid with a TiO_2 shell (Supplemental Figure 1) as described before [8, 9, 17]. Final TiO_2 concentration in this colloidal nanoparticle suspension was 200 µg/mL. Nanoparticle surface was fully covered with dopamine and the nanoparticles dialyzed in 10 mM sodium phosphate – 40 mM sodium chloride pH~4.5. Initially, nanoparticles were mixed with HeLa protein cell extracts for 16 hours at 4 °C and precipitated in order to maximize interactions between nanoparticles, proteins and protein complexes similar to immunoprecipitation approaches. Pellets consisting of nanoparticles and proteins were washed several times in protein extraction buffer; proteins that remained attached to nanoparticles after two such washes were eluted by a final wash in 2×Laemmli Buffer heated to 95 °C for 5 minutes. Eluted proteins were separated by electrophoresis (Supplemental Figure 4). Because of the high number of proteins eluted from nanoparticles, only some portions of the polyacrylamide gel were processed by mass spectrometry (Supplemental Figure 4). 252 proteins identified by this approach are listed in Supplemental Table 1. Based on bioinformatics analysis – these proteins participate in 60 DAVID annotation clusters with enrichment scores above one and up to 16 (for example, nucleotide binding sub-cluster included 114 proteins).

Three proteins were selected for further study – a cell membrane protein – transferrin receptor 1 (TfRC) which is in charge of importing transferrin, a metal binding glycoprotein, into cell [34]; a cytosolic protein – heat shock protein 90 (Hsp90) which is involved in the folding and conformational regulation of numerous client proteins and has been implicated in different cellular signaling networks (e.g., steroid hormone receptors, transcription factors and protein kinases)[35]; and a nuclear protein — poly(ADP-ribose) polymerase (PARP) which is involved in repair of single-stranded DNA breaks (SSBs) [36], regulation of chromatin structure, DNA metabolism and gene expression [37]. Paired flasks of HeLa cells seeded to reach 40 or 80% confluency overnight were treated with nanoparticles diluted to 20 µg/mL in complete medium. From the initial moment of nanoparticle treatment up to 24 hours later, pairs of nanoparticle treated cells and controls were harvested and total cellular proteins isolated using RIPA buffer and a standard processing procedure (see Methods).Previous work with non-targeted nanoparticles by our group [19] as well as others [7] has shown that non-targeted nanoparticles enter cells by every possible endocytic mechanism and that nanoparticle accumulation in cells reaches a plateau within 2 hours after treatment. Cells treated with nanoparticles and the control cells were

harvested for protein extraction immediately after nanoparticle treatment (0h timepoint) and at 1, 2, 4, 6 and 24 hours after nanoparticle treatment. Because standard protein isolation procedure includes centrifugation steps, nanoparticles present in protein extracts were precipitated and discarded in the course of the protein isolation procedure. However, because protein corona remained attached to the nanoparticles, protein supernatants from nanoparticle treated cells showed depletion of these proteins as well as proteins with decreased expression. Figure 1 shows representative Western blots for the TfRC, Hsp90 and PARP. Equal protein concentrations were loaded in each lane and Western blots for actin for each membrane were done in parallel with Western blots for protein of interest. Although actin binds to nanoparticles, we found its abundance in Western blots unchanged from lane to lane when equal amounts of proteins were loaded. We reasoned that it is possible either that actin binding to nanoparticle was less abundant when nanoparticles interacted with whole cells rather than cell lysates or that this protein has such high abundance in cells that it is difficult to deplete it. Of the three proteins tested, the quantity of Hsp90 (as much as 1% of all cell protein) appeared unchanged, similar to actin. Two other test proteins, however, showed decrease in nanoparticle treated samples. A decrease of TfRC was the most notable between 6 hours and 24 hours post-treatment. Depletion of PARP was the most pronounced and of greatest duration – no PARP was observed in any of the nanoparticle treated samples between 1-24 h after nanoparticle treatment.

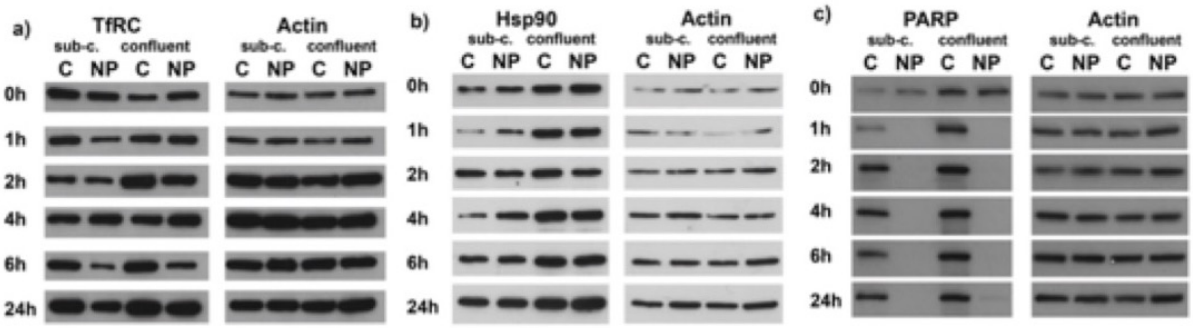

Figure 1. Protein "depletion" in nanoparticle treated samples. The quantities of TfRC (a), Hsp90 (b), and PARP (c) in whole cell lysates from nanoparticle treated and parallel control cells were evaluated by Western blots. Protein depletion in nanoparticle treated samples compared to their non-treated counterparts is most likely caused by the formation of protein corona on the surface of nanoparticles and subsequent removal of nanoparticles from the cell lysate mixtures in the course of the protein isolation procedure. Samples came from HeLa cells grown in T25 flasks to sub-confluent (sub-c.) or confluent (confluent) density and left untreated (C) or treated with nanoparticles (NP). Cells were harvested immediately (0 hours) or incubated in the presence of nanoparticles for 1, 2, 4, 6 or 24 hours before protein harvest (Western blot rows).

Considering the rapid and persistent loss of PARP from protein cell extracts of nanoparticle treated cells and the possibility that the apparent PARP decrease (and possibly TfRC changes as well) may be due to its participation in nanoparticle protein corona – we modified our protein isolation approach (see Methods). We processed pellets from protein isolation at the 2-hour timepoint like what was done when cell extracts were mixed with nanoparticles. Several washes of the pellet were done, followed by the "elution" step. Next, protein extracts, washes and eluates were probed with antibodies for TfRC, Hsp90 and PARP (Figure 2). Interestingly – while progressive washes of pellets from nanoparticle treated cells showed decreasing amounts of all three test proteins as well as actin, final elution step released a significant amount of TfRC, PARP and actin, but not Hsp90. Hsp90 may participate in nanoparticle corona, as well as several other heat shock proteins: Hsp70, Hsp60, Hsp47, shown in Supplemental Table 1, only loosely because other proteins adhering to nanoparticles appear as if though they are heat-shock denatured.

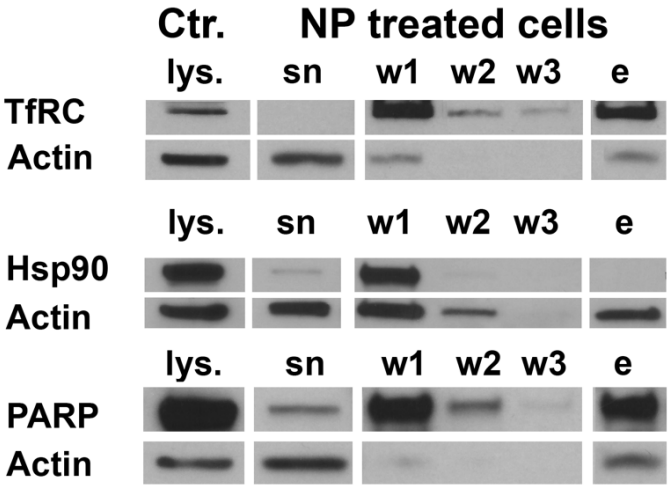

Figure 2. The protein corona accumulated on nanoparticles inside cells was stripped by sequential washes and elution steps. The first lane shows the lysate (lys.) as prepared from cells not treated with nanoparticles, followed by supernatant (sn) – cell lysate from nanoparticle treated cells obtained after centrifugation step that precipitates nanoparticles with proteins that form the corona. Nanoparticle pellets were washed and re-precipitated; each time the supernatant "wash" solution contained some of the proteins forming nanoparticle corona (w1-3). The final "elution" (e) with heating stripped some of the remaining protein corona from the nanoparticles. The proteins present in "elution" lanes were attached to the nanoparticles strongly enough to withstand room temperature washes with Laemmli buffer. These experiments were repeated three times and representative data is shown.

To explore the interaction between PARP and nanoparticles still further - we treated cells at sub-confluent density with nanoparticles for 2 hours and then exposed them to staurosporine for 4 hours at below-toxic (0.1 and 0.01μM) and toxic (1μM) concentrations. While toxic concentrations of staurosporine led to the activation of caspase 3 and subsequent PARP cleavage as expected [38], neither whole PARP nor the large cleaved fragment of PARP were present in cell lysates from cells treated with nanoparticles (Figure 3). This experiment documented that interaction between PARP and nanoparticles persists through caspase 3 activation. In addition, it is also worth noting that under these experimental conditions nanoparticles alone do not induce caspase 3 cleavage nor do they bound caspase 3.

In addition to individual protein changes in nanoparticle treated cells, we decided to explore cellular processes dependent on the concerted actions of many proteins. When we used DAVID software analysis to screen KEGG pathways that may be affected by nanoparticle protein binding (Supplemental Table 3), pathway hsa03040: Spliceosome, included the most protein members (24), while nucleotide and ribonucleotide binding topped the list of annotation clusters (enrichment score 16.54 , Supplemental Table 2).

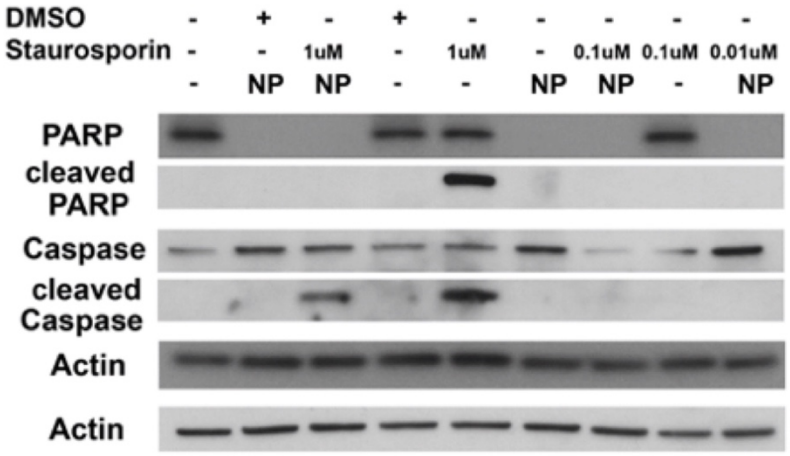

Figure 3. PARP and a large fragment of cleaved PARP are absent in Western blots of protein lysates from nanoparticle treated cells. HeLa cells were exposed to 20 μg/mL of nanoparticles for 2 hours followed by 1, 0.1 or 0.01 μM staurosporine dissolved in dimethyl sulfoxide (DMSO) for 4 hours. DMSO was used as a vehicle control. Matching pair of Western blots was done with the same protein lysates loaded in equal amounts and in the same order in both cases. Top row actin blot matches PARP blot, while bottom row actin blot corresponds to blots of cleaved PARP, caspase 3 and cleaved caspase 3. This Western Blot series is a representative example of three experiments.

With this in mind, we anticipated that the nanoparticle presence should change gene expression in general in HeLa cells treated with nanoparticles. We isolated mRNA from cells exposed to nanoparticles for 2 or 4 hours. Three biological and one technical mRNA replicates were done each for the two pairs of nanoparticle-treated and control cells were harvested at 2 or 4 hours.

Table 1. Gene expression in nanoparticle treated cells was evaluated by Illumina arrays.

			Fold Change		Adjusted p Value	
	Gene Symbol	Gene Name	2h	4h		
UPREGULATED	BLOC1S1	biogenesis of lysosomal organelles complex-1, subunit 1	1.415		0.230	
	C8orf4	chromosome 8 open reading frame 4	1.693		0.023	
	RGS2	regulator of G-protein signaling 2, 24kDa	1.424		0.205	
	DKK1	dickkopf 1 homolog (Xenopus laevis)	1.863		0.392	
	PHLDA1	pleckstrin homology-like domain, family A, member 1	2.197	1.484	0.012	0.147
	EFNA1	ephrin-A1		1.466		0.147
DOWNREGULATED	GPER	G protein-coupled estrogen receptor 1	-1.448		0.035	
	DDIT4	DNA-damage-inducible transcript 4	-1.453		0.023	
	TNFSF9	tumor necrosis factor (ligand) superfamily, member 9	-1.441		0.134	
	CA9	carbonic anhydrase IX	-1.419	-1.443	0.134	0.105
	DUSP2	dual specificity phosphatase 2	-1.425	-1.597	0.205	0.089
	HEY1	hairy/enhancer-of-split related with YRPW motif 1	-1.470	-1.489	0.044	0.031
	ID1	inhibitor of DNA binding 1, dominant negative helix-loop-helix protein	-3.473	-3.265	0.000	0.000
	ID2	inhibitor of DNA binding 2, dominant negative helix-loop-helix protein	-1.542	-1.681	0.031	0.013
	ID3	inhibitor of DNA binding 3, dominant negative helix-loop-helix protein	-2.454	-2.251	0.000	0.000
	SMAD6	SMAD family member 6	-1.488	-1.478	0.031	0.022
	TFRC	transferrin receptor (p90, CD71)	-1.481	-2.252	0.044	0.000
	NDUFA4L2	NADH dehydrogenase (ubiquinone) 1 alpha subcomplex, 4-like 2		-1.492		0.070
	PFKFB4	6-phosphofructo-2-kinase/fructose-2,6-biphosphatase 4		-1.470		0.022
	PLIN2	perilipin 2		-1.444		0.132
	CDH10	cadherin 10, type 2 (T2-cadherin)		-1.636		0.055
	DIO2	deiodinase, iodothyronine, type II		-1.442		0.028

Three biological replicates of each sample were processed by Illumina arrays. The data was subjected to ComBat [39] to remove batch effects; Limma model [40] was used for differential expression analysis; the use of these corrections resulted in adjusted p values shown. This small group of mRNAs was shown to have stable statistically significant changes in expression. Illumina array results were confirmed by real time PCR as well (Figure 4).

While RNA quality and individual array results were good (see Methods section), mRNA expression differences were subtle and batch effects could be noted for technical replicates hybridized to Illumina arrays on two separate occasions. Raw array data are available at the NIH hosted Gene Expression database (www.ncbi.nlm.nih.gov/geo/) under accession number GSE88786. A rigorous analysis was done to minimize batch differences (see Methods) and a group of 22 mRNAs was found to be consistently affected by nanoparticle treatments (Table 1). Further analysis using these 22 genes with DAVID software showed only two annotation clusters with enrichment scores better than 1 (Supplemental Table 4). Interestingly, TfRC mRNA was one of the RNAs on this listQuantitative RT-PCR (Figure 4) was done with RNA isolates prepared independently of RNAs used for microarray analyses. A a subgroup of mRNAs differentially expressed on Illumina arrays, either "robustly" according to our array post-analysis: Dual specificity phosphatase 2 (DUSP2), G protein coupled estrogen receptor (GPER), inhibitors of DNA binding 1, 2 and 3 (ID1, ID2 and ID3) and TfRC) or not. The latter group included Frizzled-9 (FZD9), mitogen activated protein kinase kinase kinase (Map3K) and single strand selective monofunctional Uracil-DNA glycosylase (SMUG1), as well as Hsp90 and PARP. While gene expression of the latter group of genes did not show changes robust enough to pass our Illumina array post-analysis, expression of many of these genes was modulated in response to nanoparticle treatments albeit mildly. It should be noted that TfRC gene expression values on Illumina array (-1.5 at 2h and -2.3 at 4h) match QRT-PCR.

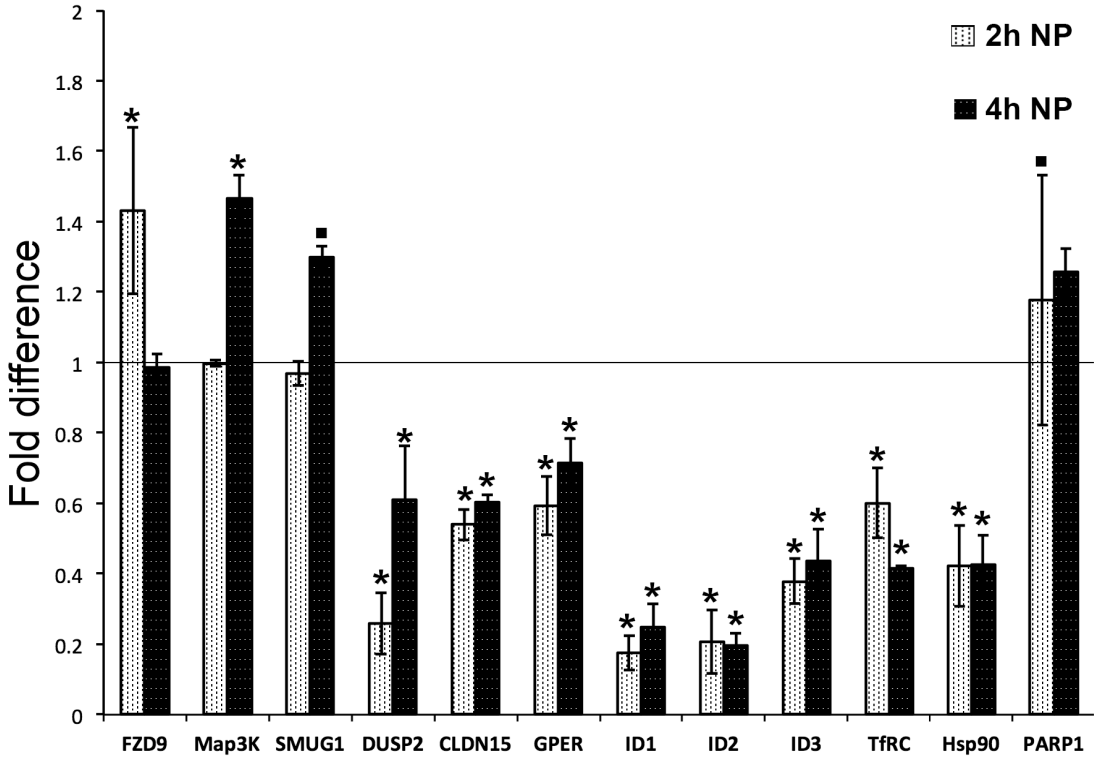

Figure 4. Quantitative real time PCR was used to corroborate the findings of Illumina microarray analysis. Gene expression after 2h or 4h of nanoparticle exposure was compared to gene expression in control cells, which was set to the value of 1 (represented by the thin horizontal line in the graph). Bars represent averages of three biological replicates (each biological replicate corresponds to three or more technical replicates by PCR), error bars show standard deviation. P values were calculated for each set of technical PCR replicates. To show statistical significance, bars with a p value less than 0.005 are labeled with an asterisk, while bar labeled with a square dot had a p value less than 0.05 in one experiment and less than 0.005 in two other experiments.

Discussion

While targeted nanoparticles often mimic different ligands (e.g. epidermal growth factor [8]) and engage suitable endocytic pathways, non-targeted nanoparticles frequently enter cells through multiple endocytic pathways [7, 19] or via GAP junctions [6]. Different endocytic mechanisms transfer nanoparticles to different subcellular compartments where they have a chance to engage in interactions with many cellular proteins. This study began with mixing nanoparticles with cell lysates. Only a portion of these proteins were analyzed, with more than 250 proteins identified (Supplemental Table 1). It is important to note that among the nanoparticle interacting proteins we found some that we have previously explored in studies with non-targeted nanoparticles (e.g. proteasome as in [16]), but none that were found in work with targeted nanoparticles [8, 28]. Three of these proteins: TfRC, Hsp90 and PARP were found also in nanoparticle protein coronas when nanoparticles were used for treatments of whole live cells in cell culture. Interestingly, retention of these proteins in nanoparticle corona varied significantly – the least stable corona participant was Hsp90 and the most stable PARP. This protein was almost completely absent from lysates of nanoparticle treated cells over period as long as 24 hours (Figure 1).

A study by Gagne and others [41] focused on discovery of proteins that are covalently poly(ADP-ribosyl)ated or bind PARP noncovalently, settled on the amino acid sequence: $[HKR]_1$- X_2- X_3- $[AQVY]_4$- $[KR]_5$- $[KR]_6$- $[AI\ LV]_7$ - $[FILPV]_8$ as a conservative version of consensus pADPr motif. Since we can note several arginine and lysine amino acids in this PARP binding sequence [41], it is possible that the numerous NH_2 groups of dopamine molecules covering the nanoparticle surface could mimic PARP binding motifs causing tight binding and depletion of this protein.

Pathway analyses were done with the list of proteins interacting with nanoparticles using tools available on the NIAID-sponsored DAVID website [42, 43]. This work suggests that many possible cellular activities may be affected by the presence of non-targeted nanoparticles. The second highest annotation cluster (enrichment score 13) points to membrane-enclosed subcellular organelles and this finding supports the concept of "universal" endocytic uptake of non-targeted nanoparticles. Remaining two of the first three annotation clusters (enrichment scores of 16 and 10) included pathways for nucleotide and ribonucleotide binding and RNA binding, spliceosome and RNA processing. Similarly, DAVID software output for KEGG pathways also listed spliceosome as one of the pathways affected by nanoparticle presence. Interestingly, mRNA changes in nanoparticle treated samples at early timepoints after nanoparticle treatment, when the relative contribution of spliceosome should be more pronounced than possible transcription associated changes, were subtle and gene expression differences rarely amounted to more than 1.5-fold.

Conclusion

In conclusion, this study shows that non-targeted nanoparticles can interact with numerous cellular proteins and impact cellular processes resulting in subtle gene expression changes. While none of the effects we find are overwhelming other cellular activities nor could be considered cytotoxic, changes occur in many cellular pathways and should be explored in combination with other cell stresses.

Conflict of Interests

The authors declare no conflicts of interest. For signed statements, please contact the journal office: editor@precisionnanomedicine.com

Acknowledgements:

This research was supported by the National Institutes of Health under the following Grant Numbers CA107467, EB002100 and U54CA119341. CURE supplement awards to the Robert H. Lurie Comprehensive Cancer Center supported B.G. P30 CA060553 - 21S1; S.M. P30 CA060553 - 20S3; and J.F. P30 CA060553 - 19S1F. F.R.Jr. was supported by funds provided by the Graduate School as part of the Summer Research Opportunity Program (SROP). The authors thank Ms. Charlene Wilke from the Biological Imaging Facility at Northwestern University for assistance in TEM imaging. Metal analysis was performed at the

Northwestern University Quantitative Bio-element Imaging Center generously supported by NASA Ames Research Center NNA06CB93G. Use of the Simpson Querrey Institute Analytical BioNanoTechnology Equipment Core (ANTEC) facility was supported by the U.S. Army Research Office, the U.S. Army Medical Research and Materiel Command, and Northwestern University funding received from the Soft and Hybrid Nanotechnology Experimental (SHyNE) Resource (NSF NNCI-1542205).

Author contributions:

R.O.L.[1], T.P.[2] and G.E.W.[3] conceived and designed the experiments; B.G.[4] S.M[5]. and R.O.L. performed RNA experiments and qPCR; F.R.[6], J.F.[7] and R.O.L. performed Western Blot experiments; L.X.[8], K.B.[9] performed nanoparticle characterization, Y.B.[10] analyzed microarray data, D.N.[11] performed mass spectrometry and analysis, S.R.[12] and M.P.[13] provided technical support and conceptual advice. R.O.L. and T.P. wrote the manuscript. G.W. supervised all the projects. All authors discussed the results and commented on the manuscript.

Quote this article as: Lastra RO, Paunesku T, Gutama B, Reyes F, Jr., François J, Martinez S, Xin L, Brown K, Zander A, Raha S, Protic M, Nanavati D, Bi YT, Woloschak GE, Protein Binding Effects of Dopamine Coated Titanium Dioxide Shell Nanoparticles, Precis. Nanomed. 2019;2(4):393-438, https://doi.org/10.33218/prnano2(4).190802.1

[1] Ruben Omar Lastra, Department of Radiation Oncology Feinberg School of Medicine, Northwestern University, Chicago, Illinois 60611, United States r-lastra@northwestern.edu
[2] Tatjana Paunesku, Department of Radiation Oncology Feinberg School of Medicine, Northwestern University, Chicago, Illinois 60611, United States, tpaunesku@northwestern.edu
[3] Gayle E Woloschak, Department of Radiation Oncology, Feinberg School of Medicine, Northwestern University, Chicago, Illinois 60611, United States, g-woloschak@northwestern.edu
[4] Barite Gutama, Present Address: Department of Chemistry, St. Olaf College, Northfield, Minnesota, 55057, United States, gutama@stolaf.edu
[5] Shelby Martinez Present Address: Department of Molecular and Cellular Biology, Harvard University, Cambridge, Massachusetts, 02138 United States, shelbymartinez@college.harvard.edu
[6] Filiberto Reyes, Jr., Present Address: School of Natural Sciences and Mathematics, California State University, Fullerton, California, 92831, United States, filyreyes@csu.fullerton.edu
[7] Josie François, Present Address: Department of Chemistry, Harvard University, Cambridge, Massachusetts, 02138 United States, jfran824@gmail.com
[8] Lun Xin[a], Present Address: Cook Pharmica LLC, Bloomington, Indiana 47403, United States, LunXin2015@u.northwestern.edu
[9] Koshonna Brown, Present Address: Daiichi Sankyo, Basking Ridge, NJ 07920, United States, kobrown@dsi.com, KoshonnaBrown2013@u.northwestern.edu
[10] Yingtao Bi, Department of Biomedical Informatics, Feinberg School of Medicine, Northwestern University, Chicago, Illinois 60611, United States, yingtao.bi@northwestern.edu
[11] Dhaval Nanavati, Present Address: AbbVie, Worcester, MA 01605, United States, d-nanavati@northwestern.edu
[12] Sumita Raha, Present Address: Rush University Medical Center, Chicago, IL 60612, United States, sumitaraha@gmail.com
[13] Miroslava Protic, Department of Radiation Oncology Feinberg School of Medicine, Northwestern University, Chicago, Illinois 60611, United States, mprotic129@gmail.com

References

[1] E. J. Petersen et al., "Identification and Avoidance of Potential Artifacts and Misinterpretations in Nanomaterial Ecotoxicity Measurements," (in English), Environmental Science & Technology, Review vol. 48, no. 8, pp. 4226-4246, Apr 2014.

[2] M. P. Monopoli, C. Aberg, A. Salvati, and K. A. Dawson, "Biomolecular coronas provide the biological identity of nanosized materials," Nat Nanotechnol, vol. 7, no. 12, pp. 779-86, Dec 2012.

[3] M. Lundqvist et al., "The evolution of the protein corona around nanoparticles: a test study," ACS Nano, vol. 5, no. 9, pp. 7503-9, Sep 27 2011.

[4] M. Karimi et al., "Smart micro/nanoparticles in stimulus-responsive drug/gene delivery systems," Chem Soc Rev, vol. 45, no. 5, pp. 1457-501, Mar 7 2016.

[5] V. Mirshafiee, M. Mahmoudi, K. Lou, J. Cheng, and M. L. Kraft, "Protein corona significantly reduces active targeting yield," Chem Commun (Camb), vol. 49, no. 25, pp. 2557-9, Mar 28 2013.

[6] M. I. Setyawati et al., "Titanium dioxide nanomaterials cause endothelial cell leakiness by disrupting the homophilic interaction of VE-cadherin," Nat Commun, vol. 4, p. 1673, 2013.

[7] E. Huerta-Garcia et al., "Internalization of titanium dioxide nanoparticles by glial cells is given at short times and is mainly mediated by actin reorganization-dependent endocytosis," Neurotoxicology, vol. 51, pp. 27-37, Dec 2015.

[8] Y. Yuan et al., "Epidermal growth factor receptor targeted nuclear delivery and high-resolution whole cell X-ray imaging of Fe3O4@TiO2 nanoparticles in cancer cells," (in eng), ACS Nano, vol. 7, no. 12, pp. 10502-17, Dec 23 2013.

[9] R. Bazak et al., "Cytotoxicity and DNA cleavage with core-shell nanocomposites functionalized by a KH domain DNA binding peptide," Nanoscale, vol. 5, no. 23, pp. 11394-9, Dec 7 2013.

[10] T. Paunesku et al., "Gadolinium-conjugated TiO2-DNA oligonucleotide nanoconjugates show prolonged intracellular retention period and T1-weighted contrast enhancement in magnetic resonance images," (in eng), Nanomedicine, vol. 4, no. 3, pp. 201-7, Sep 2008.

[11] E. M. B. Brown et al., "Methods for assessing DNA hybridization of peptide nucleic acid-titanium dioxide nanoconjugates," (in English), Analytical Biochemistry, vol. 383, no. 2, pp. 226-235, Dec 15 2008.

[12] A. G. Wu et al., "Titanium dioxide nanoparticles assembled by DNA molecules hybridization and loading of DNA interacting proteins," (in English), Nano, vol. 3, no. 1, pp. 27-36, Feb 2008.

[13] P. J. Endres, T. Paunesku, S. Vogt, T. J. Meade, and G. E. Woloschak, "DNA-TiO2 nanoconjugates labeled with magnetic resonance contrast agents," (in English), Journal of the American Chemical Society, vol. 129, no. 51, pp. 15760-+, Dec 26 2007.

[14] T. Paunesku et al., "Intracellular distribution of TiO2-DNA oligonucleotide nanoconjugates directed to nucleolus and mitochondria indicates sequence specificity," (in eng), Nano Lett, vol. 7, no. 3, pp. 596-601, Mar 2007.

[15] T. Paunesku et al., "Biology of TiO2-oligonucleotide nanocomposites," (in eng), Nat Mater, vol. 2, no. 5, pp. 343-6, May 2003.

[16] C. A. Falaschetti et al., "Negatively charged metal oxide nanoparticles interact with the 20S proteasome and differentially modulate its biologic functional effects," ACS Nano, vol. 7, no. 9, pp. 7759-72, Sep 24 2013.

[17] H. C. Arora et al., "Nanocarriers enhance Doxorubicin uptake in drug-resistant ovarian cancer cells," (in eng), Cancer Res, vol. 72, no. 3, pp. 769-78, Feb 01 2012.

[18] K. T. Thurn et al., "Labeling TiO2 nanoparticles with dyes for optical fluorescence microscopy and determination of TiO2-DNA nanoconjugate stability," (in eng), Small, vol. 5, no. 11, pp. 1318-25, Jun 2009.

[19] K. T. Thurn et al., "Endocytosis of titanium dioxide nanoparticles in prostate cancer PC-3M cells," Nanomedicine, vol. 7, no. 2, pp. 123-30, Apr 2011.

[20] T. Suzuki et al., "Genotoxicity assessment of intravenously injected titanium dioxide nanoparticles in gpt delta transgenic mice," (in eng), Mutat Res Genet Toxicol Environ Mutagen, vol. 802, pp. 30-7, May 2016.

[21] M. Reis Ede et al., "Evaluation of titanium dioxide nanocrystal-induced genotoxicity by the cytokinesis-block micronucleus assay and the Drosophila wing spot test," (in eng), Food Chem Toxicol, vol. 96, pp. 309-19, Oct 2016.

[22] C. Chakraborty, A. R. Sharma, G. Sharma, and S. S. Lee, "Zebrafish: A complete animal model to enumerate the nanoparticle toxicity," (in eng), J Nanobiotechnology, vol. 14, no. 1, p. 65, 2016.

[23] N. Asare et al., "Genotoxicity and gene expression modulation of silver and titanium dioxide nanoparticles in mice," (in eng), Nanotoxicology, vol. 10, no. 3, pp. 312-21, 2016.

[24] H. Cowie et al., "Suitability of human and mammalian cells of different origin for the assessment of genotoxicity of metal and polymeric engineered nanoparticles," (in eng), Nanotoxicology, vol. 9 Suppl 1, pp. 57-65, May 2015.

[25] C. Uboldi et al., "Role of the crystalline form of titanium dioxide nanoparticles: Rutile, and not anatase, induces toxic effects in Balb/3T3 mouse fibroblasts," (in eng), Toxicol In Vitro, vol. 31, pp. 137-45, Mar 2016.

[26] L. P. Franchi et al., "Cyto- and genotoxic effects of metallic nanoparticles in untransformed human fibroblast," (in eng), Toxicol In Vitro, vol. 29, no. 7, pp. 1319-31, Oct 2015.

[27] A. Zijno et al., "Different mechanisms are involved in oxidative DNA damage and genotoxicity induction by ZnO and TiO2 nanoparticles in human colon carcinoma cells," Toxicol In Vitro, vol. 29, no. 7, pp. 1503-12, Oct 2015.

[28] Y. Yuan et al., "Mapping the subcellular localization of FeO@TiO nanoparticles by X-ray Fluorescence Microscopy," J Phys Conf Ser, vol. 463, 2013.

[29] J. P. Holmberg, E. Ahlberg, J. Bergenholtz, M. Hassellov, and Z. Abbas, "Surface charge and interfacial potential of titanium dioxide nanoparticles: Experimental and theoretical investigations," Journal of Colloid and Interface Science, vol. 407, pp. 168-176, Oct 2013.

[30] Z. Abbas et al., "Synthesis, characterization and particle size distribution of TiO2 colloidal nanoparticles," Colloids and Surfaces a-Physicochemical and Engineering Aspects, vol. 384, no. 1-3, pp. 254-261, Jul 2011.

[31] T. Rajh, L. X. Chen, K. Lukas, T. Liu, M. C. Thurnauer, and D. M. Tiede, "Surface Restructuring of Nanoparticles: An Efficient Route for Ligand−Metal Oxide Crosstalk," The Journal of Physical Chemistry B, vol. 106, no. 41, pp. 10543-10552, 2002/10/01 2002.

[32] A. Michelmore, W. Q. Gong, P. Jenkins, and J. Ralston, "The interaction of linear polyphosphates with titanium dioxide surfaces," (in English), Physical Chemistry Chemical Physics, Article vol. 2, no. 13, pp. 2985-2992, 2000.

[33] S. E. Kim et al., "Ultrasmall nanoparticles induce ferroptosis in nutrient-deprived cancer cells and suppress tumour growth," (in Eng), Nat Nanotechnol, Sep 26 2016.

[34] A. Widera, F. Norouziyan, and W. C. Shen, "Mechanisms of TfR-mediated transcytosis and sorting in epithelial cells and applications toward drug delivery," Adv Drug Deliv Rev, vol. 55, no. 11, pp. 1439-66, Nov 14 2003.

[35] K. Terasawa, M. Minami, and Y. Minami, "Constantly updated knowledge of Hsp90," J Biochem, vol. 137, no. 4, pp. 443-7, Apr 2005.

[36] J. Morales et al., "Review of poly (ADP-ribose) polymerase (PARP) mechanisms of action and rationale for targeting in cancer and other diseases," Crit Rev Eukaryot Gene Expr, vol. 24, no. 1, pp. 15-28, 2014.

[37] L. Virag, A. Robaszkiewicz, J. M. Rodriguez-Vargas, and F. J. Oliver, "Poly(ADP-ribose) signaling in cell death," Mol Aspects Med, vol. 34, no. 6, pp. 1153-67, Dec 2013.

[38] D. W. Nicholson et al., "Identification and Inhibition of the Ice/Ced-3 Protease Necessary for Mammalian Apoptosis," (in English), Nature, vol. 376, no. 6535, pp. 37-43, Jul 6 1995.

[39] W. E. Johnson, C. Li, and A. Rabinovic, "Adjusting batch effects in microarray expression data using empirical Bayes methods," (in English), Biostatistics, vol. 8, no. 1, pp. 118-127, Jan 2007.

[40] M. E. Ritchie et al., "limma powers differential expression analyses for RNA-sequencing and microarray studies," (in English), Nucleic Acids Research, vol. 43, no. 7, Apr 20 2015.

[41] J. P. Gagne et al., "Proteome-wide identification of poly(ADP-ribose) binding proteins and poly(ADP-ribose)-associated protein complexes," (in eng), Nucleic Acids Res, vol. 36, no. 22, pp. 6959-76, Dec 2008.

[42] D. W. Huang, B. T. Sherman, and R. A. Lempicki, "Bioinformatics enrichment tools: paths toward the comprehensive functional analysis of large gene lists," (in English), Nucleic Acids Research, vol. 37, no. 1, pp. 1-13, Jan 2009.

[43] D. W. Huang, B. T. Sherman, and R. A. Lempicki, "Systematic and integrative analysis of large gene lists using DAVID bioinformatics resources," (in English), Nature Protocols, vol. 4, no. 1, pp. 44-57, 2009.

Supporting Information

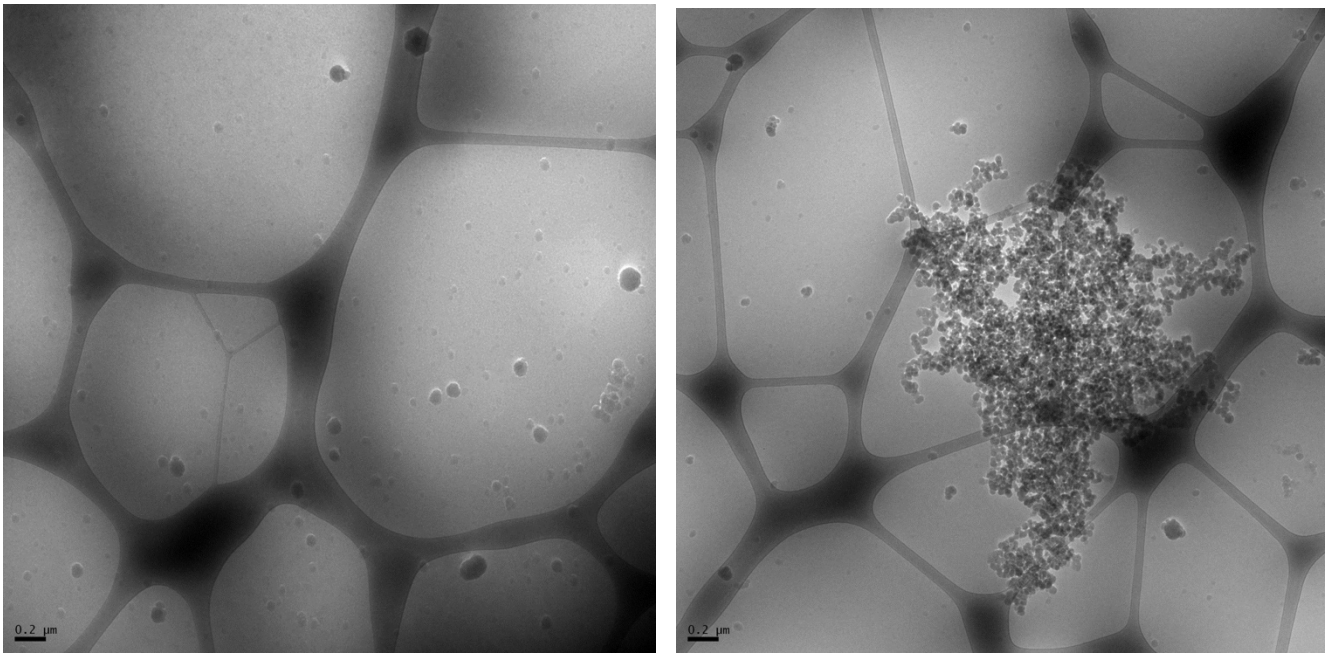

Supplemental Figure 1. Cryo TEM images of two batches of nanoparticles coated with DOPA acquired at 4000x magnification. Note that nanoparticle aggregates overall vary from few nm to 100nm. Fewer and smaller aggregates are found in recently prepared batch of nanoparticles (left) than in samples of nanoparticles coated with DOPAC more than 24 months ago (right). Experiments presented in this work were done with nanoparticles prepared within 6 months before use. Nanoparticles were diluted 1:50 with filtered dH2O, drop-cast on lacey carbon TEM grids and plunge-frozen in liquid ethane using a FEI Vitrobot. Cryo transmission electron microscopy was performed on a JEOL 1230 120 kV Transmission Electron Microscope at the Northwestern University Biological Imaging Facility.

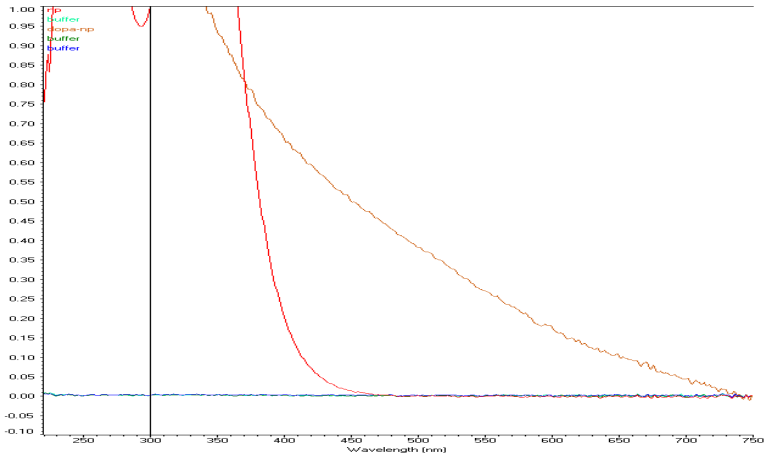

Supplemental Figure 2. UV-vis spectra of dopamine covered (brown) vs. bare (red) nanoparticles. Red shift is a characteristic change of surface coated TiO2 shell nanoparticles [1]. Studies with other nanoparticles with TiO2 surface or pure TiO2 with features smaller than 10 nm have shown that modification with catechol carrying molecules (and especially dopamine and DOPAC) is covalent and stable both "on the shelf" and inside cells [1-11]. On the other hand, binding of molecules with

single hydroxyl groups that are not arranged in catechol configuration (e.g. Adriamycin) is labile and such molecules dissociate from nanoparticles inside cells [12].

Amount of dopamine was calculated to cover nanoparticles was calculated based on molarity of nanoparticles and the number of available surface sites for this nanoparticle size (assuming average size of 10nm, calculated based on ICP-MS data and cryo-TEM sizing as previously [11, 12]). In order to ensure removal of unbound dopamine and bring the pH of the nanoparticle solution close to neutral, dopamine covered nanoparticles were dialyzed in a series of 10 mM sodium phosphate 40 mM sodium chloride buffer pH=4.5. While chloride and phosphate ions were available to neutralize NH3+ group of dopamine, it should be noted that, if any of the TiO2 molecules on nanoparticle surface were free at the type of dialysis, they could have bound to phosphates through hydrogen bonds [13].

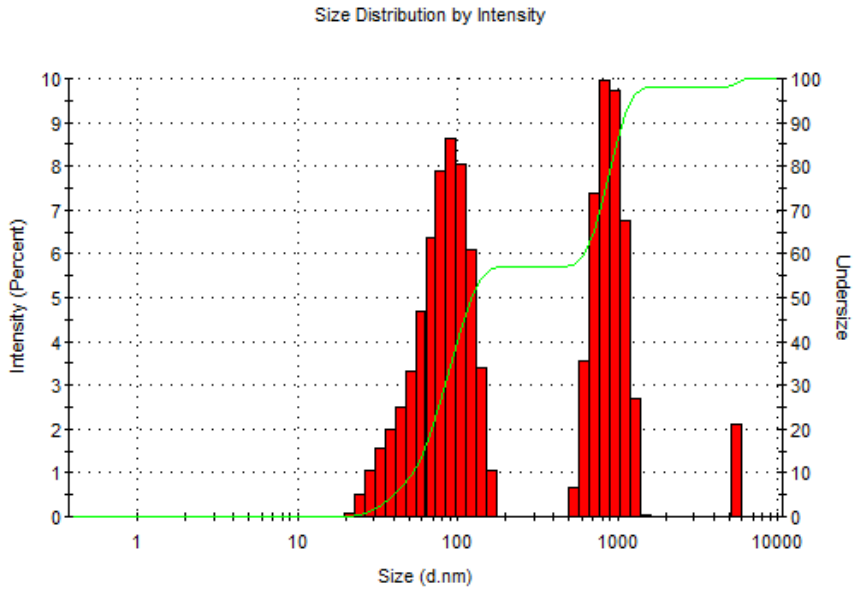

Supplemental Figure 3. Dynamic light scattering (DLS) of dopamine covered nanoparticles diluted in 10mM NaCl buffer. It should be noted that in addition to dopamine coating, these nanoparticles were also dialyzed in sodium phosphate pH=6 prior to evaluation by DLS and use in cells. This process ensured that the pH of the nanoparticle solution is close to neutral; at the same time, electropositive nanoparticle surface is partially covered by H2PO4- and HPO42- ions making the "final" nanoparticles more likely to be neutral and form aggregates. Dopamine covered nanoparticles were diluted in 10mM NaCl buffer according to the protocol recommended by the Nanotechnology Characterization Laboratory (NCL) at the National Cancer Institute (NCI). DLS measurement was done with following parameters (temp: 25°C, viscosity: 0.891, dielectric constant: 78.6, Henry function: 1.5, refractive index: 1.33) on a Zetasizer Nano (Malvern, Worcestershire, United Kingdom) housed at the ANTEC core facility, Northwestern University.

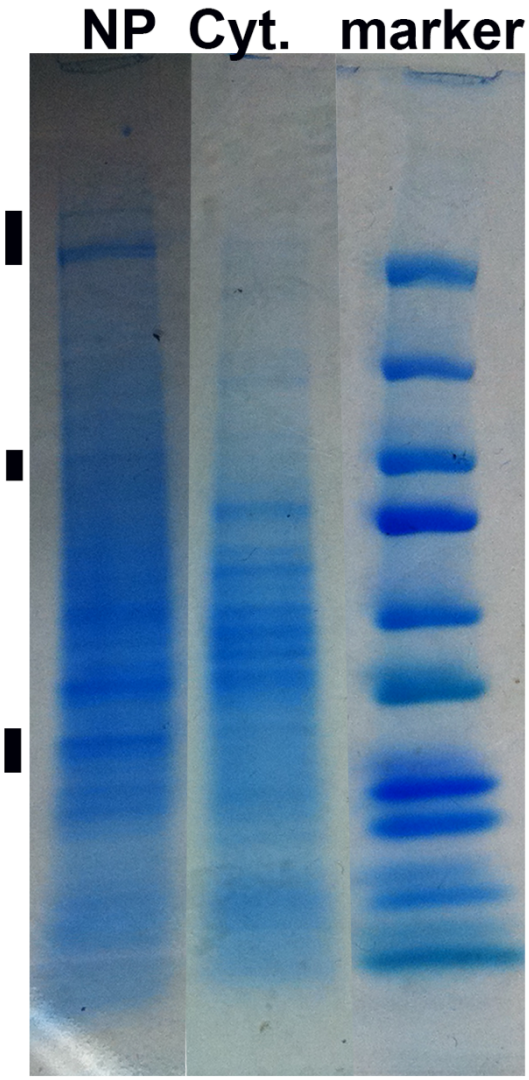

Supplemental Figure 4. Comassie stained gel showing proteins bound to nanoparticles (NP) in comparison to cytoplasmic extracts alone (Cyt.) and prior to band extraction for mass spectrometry. Black bars indicate regions close to 100 kDal, 70 kDal and 30 kDal that were selected for analysis. These areas of gel were chosen because band pattern differed most obviously from no-nanoparticle treatment lane (Cyt.). Similar approach was used to select parts of nanoparticle protein eluates from nanoparticle bound nuclear extracts.

Clarified cytoplasmic and nuclear cell protein extracts (supernatants following centrifugation) from 107 cells were mixed with 500 ul of dopamine coated nanoparticles (approximate nanoparticle molarity 18 nM) - and incubated on a slowly rotating mixer overnight. Proteins adhering to nanoparticles were collected by centrifuging the samples at 20g for 10 minutes. Pellets of nanoparticles covered with cellular protein corona were washed three times in succession with cell lysis "buffer A" and the final nanoparticle-protein pellet dissolved in gel loading Laemmli buffer and heated at 95°C for 5 minutes. Resultant mixtures were cooled, centrifuged once more and the supernatant was loaded directly onto a gel. Several areas of the gel corresponding to protein sizes 30-35 kDal, 70-75 kDal and 100-110 KDal were extracted and submitted for MS analysis. Protein identification based on peptide signatures identified by Proteome Discoverer was done against Swiss-Prot database. All identified protein signatures, from all selected gel regions from nanoparticle bound cytosolic and nuclear proteins with A(2,4) scores above 300 are listed here. Note that the proteins tested by Western blots (Hsp90, TfRC and PARP) and alpha and beta actin are featured in this list (bold).

Supplemental Table 1. Partial list of proteins adhering to dopamine-coated nanoparticles.

A(2,4) MS score	UniProtKB	Gene ID	Species	Gene Name
13795.02	B2ZZ89	802976	Homo sapiens	spectrin, beta, non-erythrocytic 1
11951.69	P06733	783039	Homo sapiens	enolase 1, (alpha)
11488.63	P78527	791583	Homo sapiens	similar to protein kinase, DNA-activated, catalytic polypeptide; protein kinase, DNA-activated, catalytic polypeptide
10943.35	Q09666	779036	Homo sapiens	AHNAK nucleoprotein
9757.37	Q5SU16	800083	Homo sapiens	tubulin, beta; similar to tubulin, beta 5; tubulin, beta pseudogene 2; tubulin, beta pseudogene 1
9642.91	Q6IPS9	821677	Homo sapiens	eukaryotic translation elongation factor 1 alpha-like 7; eukaryotic translation elongation factor 1 alpha-like 3; similar to eukaryotic translation elongation factor 1 alpha 1; eukaryotic translation elongation factor 1 alpha 1
9588.70	Q9BQE3	823156	Homo sapiens	tubulin, alpha 1c
9525.77	P68371	776899	Homo sapiens	tubulin, beta 2C
8585.34	P68366	826978	Homo sapiens	tubulin, alpha 4a
8159.81	Q13885	801263	Homo sapiens	tubulin, beta 2A
7639.81	P13639	793126	Homo sapiens	eukaryotic translation elongation factor 2
6572.82	P09651	824519	Homo sapiens	heterogeneous nuclear ribonucleoprotein A1-like 3; similar to heterogeneous nuclear ribonucleoprotein A1; heterogeneous nuclear ribonucleoprotein A1 pseudogene 2; heterogeneous nuclear ribonucleoprotein A1; heterogeneous nuclear ribonucleoprotein A1 pseudogene
5654.69	P22626	814227	Homo sapiens	heterogeneous nuclear ribonucleoprotein A2/B1
5494.99	P04264	777061	Homo sapiens	keratin 1
4987.30	Q14204	772317	Homo sapiens	dynein, cytoplasmic 1, heavy chain 1
4952.92	P13929	788559	Homo sapiens	enolase 3 (beta, muscle)
4643.86	P35527	811716	Homo sapiens	keratin 9
4372.79	P07355	787053	Homo sapiens	annexin A2 pseudogene 3; annexin A2; annexin A2 pseudogene 1
4018.94	P63261	821312	Homo sapiens	actin, gamma 1
3726.14	Q1KLZ0	777044	Homo sapiens	actin, beta
3272.78	P10809	824963	Homo sapiens	heat shock 60kDa protein 1 (chaperonin) pseudogene 5; heat shock 60kDa protein 1 (chaperonin) pseudogene 6; heat shock 60kDa protein 1 (chaperonin) pseudogene 1; heat shock 60kDa protein 1 (chaperonin) pseudogene 4; heat shock 60kDa protein 1 (chaperonin)
2983.79	Q3ZCM7	809088	Homo sapiens	tubulin, beta 8
2619.12	P13645	822924	Homo sapiens	keratin 10
2500.62	Q6ZQN2	779036	Homo sapiens	AHNAK nucleoprotein
2486.84	Q9BUF5	792713	Homo sapiens	tubulin, beta 6
2458.13	P35908	799307	Homo sapiens	keratin 2
2393.35	O15020	788928	Homo sapiens	spectrin, beta, non-erythrocytic 2
2379.81	P50454	800499	Homo sapiens	serpin peptidase inhibitor, clade H (heat shock protein 47), member 1, (collagen binding protein 1)
2205.17	P78371	819354	Homo sapiens	chaperonin containing TCP1, subunit 2 (beta)
2062.57	P30101	791817	Homo sapiens	protein disulfide isomerase family A, member 3
2055.22	Q5VTE0	821677	Homo sapiens	eukaryotic translation elongation factor 1 alpha-like 7; eukaryotic translation elongation factor 1 alpha-like 3; similar to eukaryotic translation elongation factor 1 alpha 1; eukaryotic translation elongation factor 1 alpha 1
2001.94	O75369	778146	Homo sapiens	filamin B, beta (actin binding protein 278)
1969.31	Q8WUM4	822885	Homo sapiens	programmed cell death 6 interacting protein

1960.71 P06748 810988 Homo sapiens nucleophosmin 1 (nucleolar phosphoprotein B23, numatrin) pseudogene 21; hypothetical LOC100131044; similar to nucleophosmin 1; nucleophosmin (nucleolar phosphoprotein B23, numatrin)

1873.25 Q16658 776911 Homo sapiens fascin homolog 1, actin-bundling protein (Strongylocentrotus purpuratus)

1867.63 Q5T6L4 783693 Homo sapiens argininosuccinate synthetase 1

1775.32 P07900 785761 Homo sapiens heat shock protein 90kDa alpha (cytosolic), class A member 2; heat shock protein 90kDa alpha (cytosolic), class A member 1

1753.73 P14625 804644 Homo sapiens heat shock protein 90kDa beta (Grp94), member 1

1753.42 Q53YD7 781923 Homo sapiens eukaryotic translation elongation factor 1 gamma

1634.74 A8K4W6 797595 Homo sapiens phosphoglycerate kinase 1

1615.92 P11586 784198 Homo sapiens methylenetetrahydrofolate dehydrogenase (NADP+ dependent) 1, methenyltetrahydrofolate cyclohydrolase, formyltetrahydrofolate synthetase

1595.95 Q8TBA7 785761 Homo sapiens heat shock protein 90kDa alpha (cytosolic), class A member 2; heat shock protein 90kDa alpha (cytosolic), class A member 1

1563.98 Q9UQ80 774657 Homo sapiens proliferation-associated 2G4, 38kDa; proliferation-associated 2G4 pseudogene 4

1563.02 P02786 803569 Homo sapiens transferrin receptor (p90, CD71)

1545.34 P55060 776016 Homo sapiens CSE1 chromosome segregation 1-like (yeast)

1458.93 P68363 802675 Homo sapiens hypothetical gene supported by AF081484; NM_006082; tubulin, alpha 1b

1387.95 Q14103 799658 Homo sapiens heterogeneous nuclear ribonucleoprotein D (AU-rich element RNA binding protein 1, 37kDa)

1303.14 Q9Y490 789529 Homo sapiens talin 1

1302.96 P25705 786696 Homo sapiens ATP synthase, H+ transporting, mitochondrial F1 complex, alpha subunit 1, cardiac muscle

1300.16 P51991 810069 Homo sapiens heterogeneous nuclear ribonucleoprotein A3

1298.14 P19338 792174 Homo sapiens nucleolin

1283.27 P46940 817307 Homo sapiens IQ motif containing GTPase activating protein 1

1243.69 P61978 803294 Homo sapiens heterogeneous nuclear ribonucleoprotein K; similar to heterogeneous nuclear ribonucleoprotein K

1215.13 P02538 776457 Homo sapiens keratin 6A

1209.31 Q53RC7 820046 Homo sapiens protein disulfide isomerase family A, member 6

1209.30 P00338 794884 Homo sapiens lactate dehydrogenase A

1202.92 P14618 774963 Homo sapiens similar to Pyruvate kinase, isozymes M1/M2 (Pyruvate kinase muscle isozyme) (Cytosolic thyroid hormone-binding protein) (CTHBP) (THBP1); pyruvate kinase, muscle

1192.50 Q9UBT2 824316 Homo sapiens ubiquitin-like modifier activating enzyme 2

1191.01 Q9NU22 792368 Homo sapiens MDN1, midasin homolog (yeast)

1175.06 Q13200 793113 Homo sapiens proteasome (prosome, macropain) 26S subunit, non-ATPase, 2

1105.29 P08779 799223 Homo sapiens keratin 16; keratin type 16-like

1100.73 P04406 801768 Homo sapiens glyceraldehyde-3-phosphate dehydrogenase-like 6; hypothetical protein LOC100133042; glyceraldehyde-3-phosphate dehydrogenase

1049.66 P02533 787776 Homo sapiens keratin 14

1048.19 O43175 812627 Homo sapiens phosphoglycerate dehydrogenase

1047.78 Q5T081 775327 Homo sapiens regulator of chromosome condensation 1; SNHG3-RCC1 readthrough transcript

1036.83 P48735 782325 Homo sapiens isocitrate dehydrogenase 2 (NADP+), mitochondrial

1036.01 P32754 807953 Homo sapiens 4-hydroxyphenylpyruvate dioxygenase

1025.98 Q5TZP7 804284 Homo sapiens APEX nuclease (multifunctional DNA repair enzyme) 1

1014.44 Q5U077 812048 Homo sapiens lactate dehydrogenase B
1001.55 P49411 799635 Homo sapiens Tu translation elongation factor, mitochondrial
999.69 Q99798 783221 Homo sapiens aconitase 2, mitochondrial
975.71 Q13151 782425 Homo sapiens heterogeneous nuclear ribonucleoprotein A0
954.66 Q9Y4A5 794047 Homo sapiens transformation/transcription domain-associated protein
931.47 Q9Y3F4 785208 Homo sapiens serine/threonine kinase receptor associated protein
930.96 Q1ZYQ1 814026 Homo sapiens tubulin, alpha 3d; tubulin, alpha 3c
913.26 P31943 826437 Homo sapiens heterogeneous nuclear ribonucleoprotein H1 (H)
912.91 Q14566 812967 Homo sapiens minichromosome maintenance complex component 6
910.75 P56192 818141 Homo sapiens methionyl-tRNA synthetase
896.88 P55786 810237 Homo sapiens hypothetical protein FLJ11822; aminopeptidase puromycin sensitive
876.20 P13647 808801 Homo sapiens keratin 5
867.46 Q5TZZ9 817614 Homo sapiens annexin A1
846.73 P22234 819408 Homo sapiens phosphoribosylaminoimidazole carboxylase, phosphoribosylaminoimidazole succinocarboxamide synthetase
839.87 P28838 820348 Homo sapiens leucine aminopeptidase 3
830.23 Q15645 772477 Homo sapiens thyroid hormone receptor interactor 13
822.19 B1ANK7 796931 Homo sapiens fumarate hydratase
821.74 P40121 826194 Homo sapiens capping protein (actin filament), gelsolin-like
814.61 P53618 805919 Homo sapiens coatomer protein complex, subunit beta 1
813.00 P62140 804478 Homo sapiens protein phosphatase 1, catalytic subunit, beta isoform; speedy homolog A (Xenopus laevis)
809.07 Q8NBS9 806070 Homo sapiens thioredoxin domain containing 5 (endoplasmic reticulum); muted homolog (mouse)
797.16 P09622 793209 Homo sapiens dihydrolipoamide dehydrogenase
790.57 P62136 786351 Homo sapiens protein phosphatase 1, catalytic subunit, alpha isoform
789.98 P22695 788119 Homo sapiens ubiquinol-cytochrome c reductase core protein II
782.46 Q14974 798630 Homo sapiens karyopherin (importin) beta 1
774.86 P49327 783505 Homo sapiens fatty acid synthase
771.98 A2RUM7 804383 Homo sapiens ribosomal protein L5 pseudogene 34; ribosomal protein L5 pseudogene 1; ribosomal protein L5
747.79 Q16181 807411 Homo sapiens septin 7
742.54 Q9UBB4 824796 Homo sapiens ataxin 10
741.68 Q15293 782629 Homo sapiens reticulocalbin 1, EF-hand calcium binding domain
740.01 P63010 777280 Homo sapiens adaptor-related protein complex 2, beta 1 subunit
737.50 Q9BY77 779076 Homo sapiens polymerase (DNA-directed), delta interacting protein 3
736.89 Q16881 816505 Homo sapiens thioredoxin reductase 1; hypothetical LOC100130902
736.62 Q01813 799578 Homo sapiens phosphofructokinase, platelet
731.12 Q562R1 797358 Homo sapiens actin, beta-like 2
728.43 O43592 809951 Homo sapiens exportin, tRNA (nuclear export receptor for tRNAs); similar to Exportin-T (tRNA exportin) (Exportin(tRNA))
710.83 P35250 807483 Homo sapiens replication factor C (activator 1) 2, 40kDa
699.42 Q9BQG0 805661 Homo sapiens MYB binding protein (P160) 1a
691.02 Q53TL5 776543 Homo sapiens carbamoyl-phosphate synthetase 1, mitochondrial
685.42 Q96I99 812960 Homo sapiens similar to sucb; succinate-CoA ligase, GDP-forming, beta subunit
674.03 P38919 819921 Homo sapiens eukaryotic translation initiation factor 4A, isoform 3

673.72 Q9P258 779514 Homo sapiens regulator of chromosome condensation 2
670.97 Q08J23 819340 Homo sapiens NOL1/NOP2/Sun domain family, member 2
669.99 P42765 780710 Homo sapiens hypothetical LOC648603; acetyl-Coenzyme A acyltransferase 2
668.81 P23921 795664 Homo sapiens ribonucleotide reductase M1
668.49 A8K5J1 790254 Homo sapiens uridine monophosphate synthetase
666.90 Q92769 814809 Homo sapiens histone deacetylase 2
661.28 P62195 808209 Homo sapiens proteasome (prosome, macropain) 26S subunit, ATPase, 5
650.33 Q9Y266 805698 Homo sapiens nuclear distribution gene C homolog (A. nidulans)
643.56 P06576 820161 Homo sapiens ATP synthase, H+ transporting, mitochondrial F1 complex, beta polypeptide
635.08 P08559 794862 Homo sapiens pyruvate dehydrogenase (lipoamide) alpha 1
633.49 Q9H0C8 791191 Homo sapiens integrin-linked kinase-associated serine/threonine phosphatase 2C
629.18 P48643 801908 Homo sapiens chaperonin containing TCP1, subunit 5 (epsilon)
625.87 Q10567 787777 Homo sapiens adaptor-related protein complex 1, beta 1 subunit
617.34 P45974 779174 Homo sapiens ubiquitin specific peptidase 5 (isopeptidase T)
617.19 Q15019 793629 Homo sapiens septin 2
614.36 P00505 795708 Homo sapiens glutamic-oxaloacetic transaminase 2, mitochondrial (aspartate aminotransferase 2)
614.06 P23396 816191 Homo sapiens ribosomal protein S3 pseudogene 3; ribosomal protein S3
613.21 B2R4P8 796778 Homo sapiens nascent polypeptide-associated complex alpha subunit
604.68 P24752 812798 Homo sapiens acetyl-Coenzyme A acetyltransferase 1
603.88 P00390 827002 Homo sapiens glutathione reductase
599.28 P11310 794504 Homo sapiens acyl-Coenzyme A dehydrogenase, C-4 to C-12 straight chain
594.29 P19013 783234 Homo sapiens keratin 4
586.05 P29401 809989 Homo sapiens transketolase
581.74 O14929 822025 Homo sapiens histone acetyltransferase 1
571.90 Q2Q9H2 772717 Homo sapiens glucose-6-phosphate dehydrogenase
568.86 P38159 800702 Homo sapiens similar to RNA binding motif protein, X-linked; similar to hCG2011544; RNA binding motif protein, X-linked
560.75 P78347 784409 Homo sapiens general transcription factor II, i; general transcription factor II, i, pseudogene
558.97 Q6FHQ0 784316 Homo sapiens retinoblastoma binding protein 7
557.82 P06737 804295 Homo sapiens phosphorylase, glycogen, liver
553.27 P36507 788724 Homo sapiens mitogen-activated protein kinase kinase 2 pseudogene; mitogen-activated protein kinase kinase 2
552.88 Q16543 795814 Homo sapiens cell division cycle 37 homolog (S. cerevisiae)
544.89 P22314 801917 Homo sapiens ubiquitin-like modifier activating enzyme 1
539.24 P49736 803650 Homo sapiens minichromosome maintenance complex component 2
535.75 A4QPA9 811542 Homo sapiens mitogen-activated protein kinase kinase 1
535.09 P62333 777224 Homo sapiens proteasome (prosome, macropain) 26S subunit, ATPase, 6
533.01 B2R5T5 777762 Homo sapiens protein kinase, cAMP-dependent, regulatory, type I, alpha (tissue specific extinguisher 1)
532.15 O00231 823937 Homo sapiens proteasome (prosome, macropain) 26S subunit, non-ATPase, 11
528.85 P82979 789142 Homo sapiens SAP domain containing ribonucleoprotein
525.99 Q53GA7 823156 Homo sapiens tubulin, alpha 1c

521.51 O14980 804942 Homo sapiens exportin 1 (CRM1 homolog, yeast)
521.39 B2R6Q4 782032 Homo sapiens c-src tyrosine kinase
517.61 A2ICT2 806387 Homo sapiens heat shock 70kDa protein 4-like
508.67 P29692 813345 Homo sapiens eukaryotic translation elongation factor 1 delta (guanine nucleotide exchange protein)
508.62 Q5T7Q0 816458 Homo sapiens DnaJ (Hsp40) homolog, subfamily A, member 1
502.00 Q00839 817941 Homo sapiens heterogeneous nuclear ribonucleoprotein U (scaffold attachment factor A)
500.52 Q1W6H1 789155 Homo sapiens N-methylpurine-DNA glycosylase
497.96 Q8NC51 812365 Homo sapiens SERPINE1 mRNA binding protein 1
496.85 P08238 807045 Homo sapiens heat shock protein 90kDa alpha (cytosolic), class B member 1
496.69 P11142 823976 Homo sapiens heat shock 70kDa protein 8
494.02 Q9Y678 808517 Homo sapiens coatomer protein complex, subunit gamma
493.90 P05455 781090 Homo sapiens Sjogren syndrome antigen B (autoantigen La)
491.78 P14868 778056 Homo sapiens aspartyl-tRNA synthetase
490.36 O43684 792631 Homo sapiens budding uninhibited by benzimidazoles 3 homolog (yeast)
481.63 Q53SS8 798469 Homo sapiens poly(rC) binding protein 1
480.91 P55809 793880 Homo sapiens 3-oxoacid CoA transferase 1
476.48 Q8NFW8 789123 Homo sapiens cytidine monophosphate N-acetylneuraminic acid synthetase
471.36 Q52LJ0 779142 Homo sapiens family with sequence similarity 98, member B
468.03 Q2TU77 781245 Homo sapiens similar to heat shock 70kD protein binding protein; suppression of tumorigenicity 13 (colon carcinoma) (Hsp70 interacting protein)
467.05 P41091 776090 Homo sapiens eukaryotic translation initiation factor 2, subunit 3 gamma, 52kDa
465.03 Q9ULV4 773825 Homo sapiens coronin, actin binding protein, 1C
464.94 Q99623 775357 Homo sapiens prohibitin 2
456.78 P63151 814637 Homo sapiens protein phosphatase 2 (formerly 2A), regulatory subunit B, alpha isoform
454.89 Q53XC0 815878 Homo sapiens eukaryotic translation initiation factor 2, subunit 1 alpha, 35kDa
454.54 P26599 825901 Homo sapiens polypyrimidine tract binding protein 1
448.33 P35998 799755 Homo sapiens proteasome (prosome, macropain) 26S subunit, ATPase, 2
441.52 P31153 818352 Homo sapiens methionine adenosyltransferase II, alpha
440.46 P22102 785682 Homo sapiens phosphoribosylglycinamide formyltransferase, phosphoribosylglycinamide synthetase, phosphoribosylaminoimidazole synthetase
436.30 P43490 799740 Homo sapiens nicotinamide phosphoribosyltransferase
434.64 Q32P51 813133 Homo sapiens heterogeneous nuclear ribonucleoprotein A1-like 2
432.01 Q9NR30 775290 Homo sapiens DEAD (Asp-Glu-Ala-Asp) box polypeptide 21
427.70 Q9BQ52 776933 Homo sapiens elaC homolog 2 (E. coli)
427.63 Q15233 776456 Homo sapiens non-POU domain containing, octamer-binding
427.54 P49792 823753 Homo sapiens RAN binding protein 2
426.70 Q15717 802485 Homo sapiens ELAV (embryonic lethal, abnormal vision, Drosophila)-like 1 (Hu antigen R)
426.33 Q9P289 811390 Homo sapiens serine/threonine protein kinase MST4
424.89 Q14320 791498 Homo sapiens family with sequence similarity 50, member A
423.34 P67809 788227 Homo sapiens Y box binding protein 1
419.41 P50991 801999 Homo sapiens chaperonin containing TCP1, subunit 4 (delta)
418.83 O75821 792561 Homo sapiens eukaryotic translation initiation factor 3, subunit G

417.69 Q6YN16 818917 Homo sapiens hydroxysteroid dehydrogenase like 2
416.30 P02768 803627 Homo sapiens albumin
414.59 Q86W42 820824 Homo sapiens THO complex 6 homolog (Drosophila)
413.79 O00154 806915 Homo sapiens acyl-CoA thioesterase 7
408.93 P08195 781308 Homo sapiens solute carrier family 3 (activators of dibasic and neutral amino acid transport), member 2
408.13 P13646 772288 Homo sapiens keratin 13
406.76 P27824 783822 Homo sapiens calnexin
406.00 Q9Y570 775081 Homo sapiens protein phosphatase methylesterase 1
401.13 P52597 813541 Homo sapiens heterogeneous nuclear ribonucleoprotein F
399.42 P39023 802424 Homo sapiens ribosomal protein L3; similar to 60S ribosomal protein L3 (L4)
397.69 Q9Y6E2 798384 Homo sapiens basic leucine zipper and W2 domains 2
397.09 P05556 784977 Homo sapiens integrin, beta 1 (fibronectin receptor, beta polypeptide, antigen CD29 includes MDF2, MSK12)
396.21 Q6FHX6 798249 Homo sapiens flap structure-specific endonuclease 1
396.07 P36578 786754 Homo sapiens ribosomal protein L4; ribosomal protein L4 pseudogene 5; ribosomal protein L4 pseudogene 4
393.20 P50213 786664 Homo sapiens isocitrate dehydrogenase 3 (NAD+) alpha
391.32 Q9H0S4 808234 Homo sapiens DEAD (Asp-Glu-Ala-Asp) box polypeptide 47
389.92 Q13148 789485 Homo sapiens TAR DNA binding protein
389.47 Q9Y4G6 786177 Homo sapiens talin 2
388.61 Q5JVF3 780700 Homo sapiens PCI domain containing 2
388.58 Q92785 811653 Homo sapiens D4, zinc and double PHD fingers family 2
387.27 Q08945 824758 Homo sapiens structure specific recognition protein 1
386.44 Q99986 807679 Homo sapiens vaccinia related kinase 1
380.46 P07910 784420 Homo sapiens heterogeneous nuclear ribonucleoprotein C (C1/C2)
379.89 Q5TGM6 799488 Homo sapiens FK506 binding protein 5
378.33 A8K5I0 775531 Homo sapiens heat shock 70kDa protein 1A and 70kDa hsp 1B
376.65 P11717 789007 Homo sapiens insulin-like growth factor 2 receptor
375.17 O00442 802691 Homo sapiens RNA terminal phosphate cyclase domain 1
374.15 Q02878 795791 Homo sapiens ribosomal protein L6 pseudogene 27; ribosomal protein L6 pseudogene 19; ribosomal protein L6; ribosomal protein L6 pseudogene 10
373.56 Q99832 816561 Homo sapiens chaperonin containing TCP1, subunit 7 (eta)
372.64 O14979 774982 Homo sapiens heterogeneous nuclear ribonucleoprotein D-like
369.93 O75643 778808 Homo sapiens similar to U5 snRNP-specific protein, 200 kDa; small nuclear ribonucleoprotein 200kDa (U5)
367.23 Q13838 810340 Homo sapiens HLA-B associated transcript 1
360.47 P22087 785244 Homo sapiens fibrillarin
359.98 P40937 801541 Homo sapiens replication factor C (activator 1) 5, 36.5kDa
357.99 Q01650 806504 Homo sapiens solute carrier family 7 (cationic amino acid transporter, y+ system), member 5
357.06 O00148 791596 Homo sapiens DEAD (Asp-Glu-Ala-Asp) box polypeptide 39
354.78 Q5VU21 812365 Homo sapiens SERPINE1 mRNA binding protein 1
349.00 P63092 809539 Homo sapiens GNAS complex locus
348.36 P40938 774790 Homo sapiens replication factor C (activator 1) 3, 38kDa
343.18 A1A4E9 772288 Homo sapiens keratin 13
342.62 Q6P1J9 807134 Homo sapiens cell division cycle 73, Paf1/RNA polymerase II complex component, homolog (S. cerevisiae)

338.25 Q13155 797420 Homo sapiens aminoacyl tRNA synthetase complex-interacting multifunctional protein 2; stromal antigen 3-like 3
336.07 Q14789 817861 Homo sapiens golgin B1, golgi integral membrane protein
335.13 B7Z3U6 783032 Homo sapiens ATPase, Na+/K+ transporting, alpha 1 polypeptide
334.68 Q14839 789685 Homo sapiens chromodomain helicase DNA binding protein 4
333.18 O00571 797679 Homo sapiens DEAD (Asp-Glu-Ala-Asp) box polypeptide 3, X-linked
333.04 P23526 796657 Homo sapiens adenosylhomocysteinase
329.66 P35249 778911 Homo sapiens replication factor C (activator 1) 4, 37kDa
324.63 Q96I65 803615 Homo sapiens eukaryotic translation initiation factor 4 gamma, 1
321.41 O95373 810275 Homo sapiens importin 7
321.01 P11021 815675 Homo sapiens hypothetical gene supported by AF216292; NM_005347; heat shock 70kDa protein 5 (glucose-regulated protein, 78kDa)
318.64 P56545 786688 Homo sapiens C-terminal binding protein 2
317.65 Q04637 803615 Homo sapiens eukaryotic translation initiation factor 4 gamma, 1
317.22 P05388 796227 Homo sapiens ribosomal protein, large, P0 pseudogene 2; ribosomal protein, large, P0 pseudogene 3; ribosomal protein, large, P0 pseudogene 6; ribosomal protein, large, P0
316.59 Q13813 803228 Homo sapiens spectrin, alpha, non-erythrocytic 1 (alpha-fodrin)
314.54 P36776 788157 Homo sapiens lon peptidase 1, mitochondrial
314.27 A2BF75 806428 Homo sapiens ATP-binding cassette, sub-family F (GCN20) member 1
313.51 P49454 793884 Homo sapiens centromere protein F, 350/400ka (mitosin)
311.33 Q15366 782567 Homo sapiens poly(rC) binding protein 2
307.03 P09874 806958 Homo sapiens poly (ADP-ribose) polymerase 1
306.69 P11216 779826 Homo sapiens phosphorylase, glycogen; brain
306.54 P16615 782027 Homo sapiens ATPase, Ca++ transporting, cardiac muscle, slow twitch 2
305.85 O15160 790062 Homo sapiens polymerase (RNA) I polypeptide C, 30kDa
303.48 P43246 812548 Homo sapiens mutS homolog 2, colon cancer, nonpolyposis type 1 (E. coli)

Supplemental Table 2. The list of Annotation Clusters obtained by DAVID software analysis based on the list of proteins shown in Supplemental Table 1. A partial list of proteins from HeLa cell forming the corona on dopamine coated nanoparticles. Only clusters with enrichment scores above 1 are presented here.

Annotation Cluster 1: Enrichment Score: 16.54	Count	P_Value	Benjamini
nucleotide binding	114	7.80E-30	3.90E-27
nucleotide-binding	83	5.20E-28	5.80E-26
atp-binding	64	1.30E-20	9.00E-19
purine nucleotide binding	87	3.70E-18	9.30E-16
purine ribonucleotide binding	83	4.20E-17	7.10E-15
ribonucleotide binding	83	4.20E-17	7.10E-15
adenyl nucleotide binding	71	4.10E-14	4.20E-12
purine nucleoside binding	71	8.80E-14	7.40E-12
nucleoside binding	71	1.20E-13	8.90E-12
adenyl ribonucleotide binding	67	4.10E-13	2.60E-11
ATP binding	66	7.10E-13	4.00E-11
nucleotide phosphate-binding region:ATP	37	6.50E-09	2.80E-06

Annotation Cluster 2: Enrichment Score: 13.07	Count	P_Value	Benjamini
membrane-enclosed lumen	82	1.30E-17	2.00E-15
intracellular organelle lumen	80	1.50E-17	1.50E-15
organelle lumen	81	1.50E-17	1.20E-15
nuclear lumen	57	1.10E-09	3.70E-08
nucleoplasm	36	1.40E-06	4.10E-05

Annotation Cluster 3: Enrichment Score: 10.02	Count	P_Value	Benjamini
rna-binding	43	2.10E-21	1.70E-19
RNA binding	49	4.20E-16	5.60E-14
ribonucleoprotein complex	40	1.30E-15	8.30E-14
heterogeneous nuclear ribonucleoprotein complex	11	2.50E-14	1.30E-12
ribonucleoprotein	23	9.80E-12	4.20E-10
RRM	19	1.80E-11	1.30E-09
mrna splicing	20	2.30E-11	8.60E-10
domain:RRM 1	14	5.20E-10	4.60E-07
domain:RRM 2	14	5.20E-10	4.60E-07
mrna processing	20	9.70E-10	2.30E-08
mRNA metabolic process	27	1.00E-09	7.70E-07
nuclear mRNA splicing, via spliceosome	18	1.00E-09	5.10E-07
RNA splicing, via transesterification reactions with bulged adenosine as nucleophile	18	1.00E-09	5.10E-07
RNA splicing, via transesterification reactions	18	1.00E-09	5.10E-07
RNA recognition motif, RNP-1	19	1.70E-09	2.60E-07
Nucleotide-binding, alpha-beta plait	19	2.00E-09	2.40E-07

RNA splicing	23	3.60E-09	1.30E-06
Spliceosome	14	4.20E-09	9.50E-08
RNA processing	31	1.70E-08	5.00E-06
mRNA processing	23	3.40E-08	7.10E-06
spliceosome	14	3.10E-07	9.80E-06
Spliceosome	13	8.90E-05	2.80E-03
Annotation Cluster 4: Enrichment Score: 9.36	Count	P_Value	Benjamini
non-membrane-bounded organelle	89	2.10E-12	8.20E-11
intracellular non-membrane-bounded organelle	89	2.10E-12	8.20E-11
cytoskeleton	45	1.80E-05	3.60E-04
Annotation Cluster 5: Enrichment Score: 7.99	Count	P_Value	Benjamini
heterogeneous nuclear ribonucleoprotein complex	11	2.50E-14	1.30E-12
methylation	20	2.90E-10	8.90E-09
domain:RRM 1	14	5.20E-10	4.60E-07
domain:RRM 2	14	5.20E-10	4.60E-07
PIRSF002072:helix-destabilizing protein	6	6.50E-07	4.90E-05
compositionally biased region:Gly-rich	15	2.40E-06	2.10E-04
domain:RRM 3	5	3.80E-03	1.00E-01
Annotation Cluster 6: Enrichment Score: 7.62	Count	P_Value	Benjamini
ATPase activity	26	8.70E-10	3.40E-08
AAA	14	7.40E-09	2.60E-07
ATPase, AAA+ type, core	14	1.70E-07	1.70E-05
ATPase activity, coupled	20	3.00E-07	1.10E-05
Annotation Cluster 7: Enrichment Score: 7.31	Count	P_Value	Benjamini
melanosome	18	8.80E-14	3.90E-12
pigment granule	18	8.80E-14	3.90E-12
cytoplasmic membrane-bounded vesicle	25	1.70E-05	3.50E-04
membrane-bounded vesicle	25	2.80E-05	4.90E-04
vesicle	27	5.50E-05	8.90E-04
cytoplasmic vesicle	26	7.30E-05	1.10E-03
Annotation Cluster 8: Enrichment Score: 6.78	Count	P_Value	Benjamini
isopeptide bond	21	4.90E-09	1.00E-07
ubl conjugation	25	5.20E-07	7.90E-06
cross-link:Glycyl lysine isopeptide (Lys-Gly) (inter-chain with G-Cter in ubiquitin)	14	1.80E-06	1.90E-04
Annotation Cluster 9: Enrichment Score: 6.06	Count	P_Value	Benjamini
protein biosynthesis	18	2.90E-10	8.20E-09

translation	20	4.40E-06	3.20E-04
translational elongation	11	8.90E-06	5.30E-04
translation factor activity, nucleic acid binding	10	5.30E-05	1.40E-03

Annotation Cluster 10: Enrichment Score: 6.03	Count	P_Value	Benjamini
Chaperone	20	1.50E-13	7.30E-12
unfolded protein binding	18	1.40E-11	6.40E-10
molecular chaperone	6	3.70E-07	6.00E-06
protein folding	16	3.90E-07	5.20E-05
stress response	7	1.90E-04	1.60E-03
response to unfolded protein	8	2.10E-04	8.30E-03
response to protein stimulus	8	2.40E-03	5.30E-02
Antigen processing and presentation	7	2.00E-02	2.10E-01

Annotation Cluster 11: Enrichment Score: 5.82	Count	P_Value	Benjamini
generation of precursor metabolites and energy	26	1.50E-10	2.30E-07
cellular carbohydrate catabolic process	13	2.10E-08	5.20E-06
glycolysis	9	7.10E-08	1.30E-06
carbohydrate catabolic process	13	3.50E-07	5.80E-05
glucose metabolic process	15	3.70E-07	5.50E-05
glucose catabolic process	10	5.60E-07	6.90E-05
glycolysis	9	1.20E-06	1.30E-04
hexose catabolic process	10	2.50E-06	2.40E-04
monosaccharide catabolic process	10	3.20E-06	2.70E-04
hexose metabolic process	15	5.70E-06	4.00E-04
alcohol catabolic process	10	9.80E-06	5.40E-04
Glycolysis / Gluconeogenesis	10	2.00E-05	8.20E-04
monosaccharide metabolic process	15	2.90E-05	1.40E-03
binding site:Substrate	15	3.00E-05	2.20E-03
Pyruvate metabolism	6	3.50E-03	5.30E-02

Annotation Cluster 12: Enrichment Score: 5.39	Count	P_Value	Benjamini
structural molecule activity	37	3.30E-10	1.40E-08
cytoskeleton	45	1.80E-05	3.60E-04
cytoskeletal part	35	2.00E-05	3.70E-04
microtubule cytoskeleton	20	2.20E-03	2.50E-02

Annotation Cluster 13: Enrichment Score: 5.18	Count	P_Value	Benjamini
Tubulin/FtsZ, 2-layer sandwich domain	9	4.60E-10	2.70E-07
Tubulin, conserved site	9	6.90E-10	2.00E-07
Tubulin/FtsZ, GTPase domain	9	1.00E-09	2.00E-07
Tubulin	9	1.00E-09	2.00E-07
PIRSF002306:tubulin	9	1.40E-08	2.10E-06

Pathogenic Escherichia coli infection	13	1.50E-08	1.90E-06
cellular protein complex assembly	16	1.20E-07	2.20E-05
protein polymerization	9	1.60E-06	1.70E-04
protein complex assembly	26	1.90E-06	1.90E-04
protein complex biogenesis	26	1.90E-06	1.90E-04
gtp-binding	17	5.10E-06	6.30E-05
nucleotide phosphate-binding region:GTP	16	6.30E-06	5.00E-04
cellular macromolecular complex assembly	19	9.50E-06	5.40E-04
Beta tubulin	5	1.30E-05	7.70E-04
Gap junction	12	1.50E-05	9.70E-04
microtubule-based movement	11	2.40E-05	1.30E-03
macromolecular complex assembly	28	2.80E-05	1.40E-03
cellular macromolecular complex subunit organization	19	4.40E-05	2.10E-03
macromolecular complex subunit organization	28	8.60E-05	3.70E-03
GTPase activity	14	8.70E-05	2.10E-03
Beta tubulin, autoregulation binding site	5	1.10E-04	5.00E-03
microtubule	12	1.90E-04	1.60E-03
GTP binding	7	2.00E-04	1.70E-03
Alpha tubulin	4	2.40E-04	9.20E-03
GTP binding	17	8.60E-04	1.50E-02
guanyl ribonucleotide binding	17	1.10E-03	1.90E-02
guanyl nucleotide binding	17	1.10E-03	1.90E-02
microtubule-based process	13	1.40E-03	3.60E-02
microtubule cytoskeleton	20	2.20E-03	2.50E-02
microtubule	13	2.30E-03	2.50E-02
Annotation Cluster 14: Enrichment Score: 4.2	Count	P_Value	Benjamini
nucleocytoplasmic transport	14	2.80E-06	2.50E-04
nuclear transport	14	3.30E-06	2.50E-04
nucleic acid transport	11	6.20E-06	4.20E-04
RNA transport	11	6.20E-06	4.20E-04
establishment of RNA localization	11	6.20E-06	4.20E-04
RNA localization	11	8.10E-06	5.00E-04
nucleobase, nucleoside, nucleotide and nucleic acid transport	11	2.40E-05	1.30E-03
mRNA transport	7	3.50E-04	2.60E-03
nuclear export	7	5.50E-04	1.80E-02
RNA export from nucleus	6	6.40E-04	2.00E-02
mRNA transport	8	7.30E-04	2.10E-02
mRNA export from nucleus	3	1.10E-01	6.10E-01
Annotation Cluster 15: Enrichment Score: 4.11	Count	P_Value	Benjamini
structural constituent of cytoskeleton	16	2.00E-12	1.00E-10

region of interest:Coil 2	10	1.20E-07	3.40E-05
region of interest:Linker 12	10	1.20E-07	3.40E-05
region of interest:Coil 1B	10	2.60E-07	5.60E-05
region of interest:Coil 1A	10	2.60E-07	5.60E-05
region of interest:Linker 1	10	2.60E-07	5.60E-05
region of interest:Rod	10	2.90E-07	5.10E-05
region of interest:Head	10	3.70E-07	5.40E-05
region of interest:Tail	10	4.70E-07	5.90E-05
Intermediate filament	10	6.30E-07	9.20E-06
PIRSF002282:cytoskeletal keratin	10	7.80E-06	3.90E-04
Filament	9	9.20E-06	6.80E-04
Intermediate filament protein, conserved site	9	9.20E-06	6.80E-04
Intermediate filament protein	9	1.00E-05	6.70E-04
site:Stutter	6	5.80E-05	3.60E-03
palmoplantar keratoderma	5	8.40E-05	8.90E-04
keratin	10	9.40E-05	9.70E-04
ectoderm development	12	6.50E-04	2.00E-02
keratin filament	8	6.70E-04	9.00E-03
Keratin, type I	5	1.30E-03	3.00E-02
epidermis development	11	1.30E-03	3.30E-02
intermediate filament	10	3.70E-03	3.50E-02
intermediate filament cytoskeleton	10	4.30E-03	3.90E-02
Type II keratin	4	7.50E-03	1.30E-01
intermediate filament cytoskeleton organization	3	4.50E-02	4.00E-01
intermediate filament-based process	3	5.40E-02	4.30E-01
epithelial cell differentiation	6	8.70E-02	5.50E-01
keratinocyte differentiation	3	3.10E-01	8.90E-01
epithelium development	6	3.50E-01	9.10E-01
epidermal cell differentiation	3	3.50E-01	9.10E-01
coiled coil	21	9.00E-01	1.00E+00

Annotation Cluster 16: Enrichment Score: 3.88	Count	P_Value	Benjamini
Chaperone, tailless complex polypeptide 1	5	1.30E-05	7.70E-04
Chaperonin Cpn60/TCP-1	5	5.10E-05	2.70E-03
chaperonin-containing T-complex	4	1.50E-04	2.20E-03
Chaperonin TCP-1, conserved site	4	3.30E-04	1.10E-02
PIRSF002584:molecular chaperone t-complex-type	4	1.20E-03	3.60E-02

Annotation Cluster 17: Enrichment Score: 3.73	Count	P_Value	Benjamini
cofactor binding	18	1.80E-06	6.00E-05
NAD or NADH binding	8	1.60E-05	4.70E-04
NAD(P)-binding domain	11	6.60E-05	3.20E-03
coenzyme binding	13	8.10E-05	2.00E-03

nad	11	1.60E-04	1.40E-03
oxidoreductase	19	3.20E-04	2.50E-03
binding site:NAD	6	4.30E-04	1.90E-02
nucleotide phosphate-binding region:NAD	6	2.90E-03	8.90E-02
oxidation reduction	19	2.70E-02	2.90E-01
Annotation Cluster 18: Enrichment Score: 3.28	Count	P_Value	Benjamini
energy derivation by oxidation of organic compounds	13	6.90E-06	4.40E-04
Citrate cycle (TCA cycle)	7	1.20E-04	2.90E-03
tricarboxylic acid cycle	5	1.30E-04	1.20E-03
acetyl-CoA metabolic process	6	1.70E-04	6.90E-03
aerobic respiration	6	3.00E-04	1.20E-02
coenzyme metabolic process	11	3.10E-04	1.20E-02
acetyl-CoA catabolic process	5	5.80E-04	1.90E-02
tricarboxylic acid cycle	5	5.80E-04	1.90E-02
coenzyme catabolic process	5	9.40E-04	2.60E-02
cofactor catabolic process	5	1.80E-03	4.30E-02
cofactor metabolic process	11	2.00E-03	4.50E-02
cellular respiration	7	6.40E-03	1.10E-01
dicarboxylic acid metabolic process	4	2.00E-02	2.30E-01
Annotation Cluster 19: Enrichment Score: 3.26	Count	P_Value	Benjamini
translation factor activity, nucleic acid binding	10	5.30E-05	1.40E-03
elongation factor	5	1.30E-04	1.20E-03
translation elongation factor activity	5	7.30E-04	1.40E-02
Translation elongation factor EFTu/EF1A, domain 2	4	1.20E-03	3.00E-02
Protein synthesis factor, GTP-binding	4	1.80E-03	4.00E-02
eukaryotic translation elongation factor 1 complex	3	2.70E-03	2.80E-02
Annotation Cluster 20: Enrichment Score: 2.98	Count	P_Value	Benjamini
regulation of mRNA stability	5	4.80E-04	1.70E-02
regulation of RNA stability	5	6.80E-04	2.10E-02
RNA stabilization	4	1.90E-03	4.50E-02
mRNA stabilization	4	1.90E-03	4.50E-02
Annotation Cluster 21: Enrichment Score: 2.93	Count	P_Value	Benjamini
dna replication	9	1.60E-05	1.90E-04
PIRSF004274:phage T4 DNA polymerase accessory protein 44	4	4.40E-05	1.70E-03
DNA clamp loader activity	4	5.10E-05	1.40E-03
protein-DNA loading ATPase activity	4	5.10E-05	1.40E-03
DNA replication factor C complex	4	8.90E-05	1.30E-03
DNA replication	7	2.80E-04	5.80E-03

Replication factor C	3	6.20E-04	1.90E-02
DNA replication	11	1.60E-03	4.00E-02
replication fork	5	1.90E-03	2.30E-02
Mismatch repair	5	2.60E-03	4.60E-02
DNA strand elongation during DNA replication	3	2.80E-03	6.10E-02
nucleotide-excision repair, DNA gap filling	4	2.80E-03	6.00E-02
DNA strand elongation	3	4.20E-03	8.20E-02
DNA-dependent DNA replication	5	1.70E-02	2.10E-01
DNA-dependent ATPase activity	5	1.70E-02	2.00E-01
nucleotide-excision repair	4	6.80E-02	4.90E-01
Nucleotide excision repair	4	1.10E-01	5.40E-01

Annotation Cluster 22: Enrichment Score: 2.92	Count	P_Value	Benjamini
repeat:1-2	5	3.10E-04	1.50E-02
repeat:1-1	5	3.60E-04	1.60E-02
repeat:2-1	4	3.80E-03	1.00E-01
repeat:2-2	4	4.80E-03	1.20E-01

Annotation Cluster 23: Enrichment Score: 2.88	Count	P_Value	Benjamini
ATPase activity, coupled	20	3.00E-07	1.10E-05
short sequence motif:Q motif	6	1.00E-04	5.50E-03
RNA helicase, DEAD-box type, Q motif	6	1.80E-04	7.60E-03
HELICc	8	1.90E-04	4.60E-03
DEXDc	8	2.30E-04	4.10E-03
DNA/RNA helicase, DEAD/DEAH box type, N-terminal	7	2.50E-04	9.00E-03
ATP-dependent RNA helicase activity	5	4.30E-04	8.70E-03
RNA-dependent ATPase activity	5	5.20E-04	1.00E-02
Helicase, superfamily 1 and 2, ATP-binding	8	9.30E-04	2.70E-02
DNA/RNA helicase, C-terminal	8	9.30E-04	2.70E-02
DEAD-like helicase, N-terminal	8	1.00E-03	2.70E-02
RNA helicase activity	5	1.50E-03	2.50E-02
helicase	8	1.60E-03	1.10E-02
purine NTP-dependent helicase activity	8	1.60E-03	2.60E-02
ATP-dependent helicase activity	8	1.60E-03	2.60E-02
domain:Helicase C-terminal	7	2.30E-03	7.70E-02
domain:Helicase ATP-binding	7	2.90E-03	8.60E-02
helicase activity	9	3.20E-03	4.60E-02
PIRSF003023:translation initiation factor eIF-4A	3	4.80E-03	1.20E-01
RNA helicase, ATP-dependent, DEAD-box, conserved site	4	1.10E-02	1.70E-01
short sequence motif:DEAD box	3	6.60E-02	6.90E-01
nuclear speck	4	2.50E-01	6.80E-01

nuclear body	5	3.10E-01	7.50E-01
Annotation Cluster 24: Enrichment Score: 2.49	Count	P_Value	Benjamini
cell cortex	10	7.80E-04	1.00E-02
cell cortex part	7	2.70E-03	2.80E-02
cytoskeleton	16	1.60E-02	6.90E-02
Annotation Cluster 25: Enrichment Score: 2.39	Count	P_Value	Benjamini
cytosolic part	14	1.60E-06	4.10E-05
translational elongation	11	8.90E-06	5.30E-04
ribosome	6	2.30E-03	1.50E-02
cytosolic large ribosomal subunit	5	3.60E-03	3.60E-02
large ribosomal subunit	6	5.20E-03	4.70E-02
cytosolic ribosome	6	1.20E-02	8.40E-02
ribosomal subunit	7	2.10E-02	1.30E-01
ribosome	9	2.80E-02	1.60E-01
Ribosome	6	7.50E-02	4.30E-01
ribosomal protein	6	9.20E-02	3.00E-01
structural constituent of ribosome	6	1.70E-01	7.70E-01
Annotation Cluster 26: Enrichment Score: 2.38	Count	P_Value	Benjamini
mitochondrial matrix	16	6.40E-06	1.40E-04
mitochondrial lumen	16	6.40E-06	1.40E-04
transit peptide	20	1.10E-05	1.40E-04
transit peptide:Mitochondrion	19	3.40E-05	2.30E-03
Citrate cycle (TCA cycle)	7	1.20E-04	2.90E-03
mitochondrion	22	2.20E-03	1.40E-02
mitochondrial part	19	1.10E-02	8.30E-02
mitochondrion	28	2.50E-02	1.40E-01
organelle envelope	18	3.10E-02	1.60E-01
envelope	18	3.20E-02	1.70E-01
mitochondrial inner membrane	9	1.40E-01	5.10E-01
organelle inner membrane	9	1.90E-01	6.00E-01
mitochondrial membrane	9	3.40E-01	7.80E-01
mitochondrial envelope	9	4.00E-01	8.40E-01
organelle membrane	19	5.70E-01	9.30E-01
Annotation Cluster 27: Enrichment Score: 2.32	Count	P_Value	Benjamini
cell cycle	30	6.30E-05	2.90E-03
mitotic cell cycle	19	7.00E-05	3.10E-03
cell cycle process	24	1.10E-04	4.60E-03
mitosis	10	5.60E-04	4.10E-03
mitosis	11	4.70E-03	9.00E-02

nuclear division	11	4.70E-03	9.00E-02
M phase of mitotic cell cycle	11	5.30E-03	9.40E-02
organelle fission	11	6.20E-03	1.00E-01
cell division	10	6.70E-03	3.70E-02
M phase	13	1.10E-02	1.60E-01
cell cycle phase	15	1.20E-02	1.60E-01
cell cycle	13	1.50E-02	6.70E-02
cell division	9	1.40E-01	6.70E-01
chromosome, centromeric region	5	1.50E-01	5.30E-01
spindle	5	2.30E-01	6.60E-01

Annotation Cluster 28: Enrichment Score: 2.29	Count	P_Value	Benjamini
allosteric enzyme	6	1.30E-04	1.20E-03
energy reserve metabolic process	6	8.00E-04	2.30E-02
cellular polysaccharide metabolic process	6	2.10E-03	4.60E-02
glycogen metabolism	4	2.60E-03	1.60E-02
glycogen metabolic process	5	2.90E-03	6.00E-02
glucan metabolic process	5	3.20E-03	6.60E-02
cellular glucan metabolic process	5	3.20E-03	6.60E-02
glycogen catabolic process	3	4.20E-03	8.20E-02
cellular polysaccharide catabolic process	3	5.80E-03	9.90E-02
glucan catabolic process	3	5.80E-03	9.90E-02
carbohydrate metabolism	5	1.60E-02	7.00E-02
polysaccharide metabolic process	6	4.20E-02	3.80E-01
Insulin signaling pathway	8	6.10E-02	4.10E-01
polysaccharide catabolic process	3	8.30E-02	5.40E-01

Annotation Cluster 29: Enrichment Score: 2.29	Count	P_Value	Benjamini
translation factor activity, nucleic acid binding	10	5.30E-05	1.40E-03
Initiation factor	4	2.80E-02	1.10E-01
translation initiation factor activity	4	9.10E-02	5.90E-01

Annotation Cluster 30: Enrichment Score: 2.28	Count	P_Value	Benjamini
short sequence motif:Prevents secretion from ER	7	1.00E-04	5.30E-03
Redox-active center	6	1.80E-04	1.60E-03
Endoplasmic reticulum, targeting sequence	6	4.60E-04	1.50E-02
cell redox homeostasis	7	7.20E-04	2.10E-02
endoplasmic reticulum lumen	7	2.20E-03	2.60E-02
Disulphide isomerase	3	3.00E-03	6.10E-02
domain:Thioredoxin 2	3	5.50E-03	1.40E-01
domain:Thioredoxin 1	3	5.50E-03	1.40E-01
Thioredoxin-like subdomain	3	8.70E-03	1.40E-01
PIRSF001487:protein disulfide-isomerase	3	9.90E-03	1.90E-01

ER-Golgi intermediate compartment	4	3.10E-02	1.70E-01
Thioredoxin, conserved site	3	5.40E-02	5.30E-01
Thioredoxin domain	3	5.80E-02	5.50E-01
Thioredoxin fold	5	5.90E-02	5.50E-01
Thioredoxin-like	3	9.50E-02	6.80E-01
Annotation Cluster 31: Enrichment Score: 2.18	Count	P_Value	Benjamini
DNA metabolic process	20	1.20E-03	3.10E-02
cellular response to stress	21	1.80E-03	4.20E-02
DNA repair	13	3.70E-03	7.30E-02
response to DNA damage stimulus	15	5.10E-03	9.10E-02
dna repair	8	1.10E-02	5.40E-02
DNA damage	8	1.60E-02	6.90E-02
base-excision repair	3	7.80E-02	5.30E-01
Annotation Cluster 32: Enrichment Score: 2.16	Count	P_Value	Benjamini
nucleocytoplasmic transport	14	2.80E-06	2.50E-04
nuclear transport	14	3.30E-06	2.50E-04
intracellular transport	25	3.90E-04	1.40E-02
domain:Importin N-terminal	4	6.70E-04	2.80E-02
nuclear import	8	7.80E-04	2.20E-02
Importin-beta, N-terminal	4	1.20E-03	3.00E-02
Armadillo-like helical	8	2.60E-03	5.50E-02
protein import into nucleus, docking	4	2.80E-03	6.00E-02
protein import into nucleus	7	3.60E-03	7.20E-02
protein localization in nucleus	7	5.50E-03	9.60E-02
nuclear pore	6	1.00E-02	8.00E-02
protein transporter activity	6	1.80E-02	2.10E-01
pore complex	6	2.20E-02	1.30E-01
nuclear envelope	9	2.20E-02	1.30E-01
protein import	7	2.50E-02	2.80E-01
intracellular protein transport	13	2.80E-02	3.00E-01
protein localization in organelle	7	4.00E-02	3.70E-01
cellular protein localization	13	5.10E-02	4.20E-01
cellular macromolecule localization	13	5.30E-02	4.30E-01
endomembrane system	20	6.60E-02	3.00E-01
protein targeting	8	7.70E-02	5.30E-01
protein localization	22	7.90E-02	5.30E-01
protein transport	11	9.00E-02	3.00E-01
protein transport	19	1.00E-01	6.00E-01
establishment of protein localization	19	1.10E-01	6.20E-01
Annotation Cluster 33: Enrichment Score: 1.85	Count	P_Value	Benjamini
posttranscriptional regulation of gene expression	12	1.00E-03	2.80E-02

translation regulation	5	1.00E-02	5.10E-02
regulation of translation	5	2.10E-01	8.00E-01
Annotation Cluster 35: Enrichment Score: 1.88	Count	P_Value	Benjamini
coenzyme metabolic process	11	3.10E-04	1.20E-02
cellular amide metabolic process	7	3.80E-04	1.40E-02
cofactor metabolic process	11	2.00E-03	4.50E-02
nicotinamide metabolic process	4	3.10E-02	3.10E-01
nicotinamide nucleotide metabolic process	4	3.10E-02	3.10E-01
alkaloid metabolic process	4	3.30E-02	3.20E-01
pyridine nucleotide metabolic process	4	3.50E-02	3.40E-01
oxidoreduction coenzyme metabolic process	4	6.00E-02	4.50E-01
NAD metabolic process	3	6.80E-02	4.90E-01
secondary metabolic process	4	1.50E-01	7.10E-01
Annotation Cluster 35: Enrichment Score: 1.85	Count	P_Value	Benjamini
maintenance of location	6	4.80E-03	9.00E-02
cytoskeletal anchoring at plasma membrane	3	7.70E-03	1.20E-01
maintenance of location in cell	5	9.10E-03	1.40E-01
maintenance of protein location in cell	4	3.30E-02	3.20E-01
maintenance of protein location	4	4.90E-02	4.10E-01
Annotation Cluster 36: Enrichment Score: 1.83	Count	P_Value	Benjamini
redox-active disulfide	4	1.10E-04	1.10E-03
Redox-active center	6	1.80E-04	1.60E-03
cell redox homeostasis	7	7.20E-04	2.10E-02
Mercuric reductase	3	2.00E-03	4.50E-02
Pyridine nucleotide-disulphide oxidoreductase, class I, active site	3	2.00E-03	4.50E-02
Pyridine nucleotide-disulphide oxidoreductase, dimerisation	3	5.50E-03	1.00E-01
Pyridine nucleotide-disulphide oxidoreductase, NAD-binding region	3	7.00E-03	1.30E-01
oxidoreductase activity, acting on sulfur group of donors, NAD or NADP as acceptor	3	1.00E-02	1.30E-01
FAD-dependent pyridine nucleotide-disulphide oxidoreductase	3	3.00E-02	3.60E-01
nucleotide phosphate-binding region:FAD	4	4.30E-02	5.60E-01
Flavoprotein	5	4.70E-02	1.80E-01
Thioredoxin fold	5	5.90E-02	5.50E-01
FAD binding	4	1.30E-01	6.90E-01
oxidoreductase activity, acting on sulfur group of donors	3	1.50E-01	7.30E-01
FAD	4	1.80E-01	5.00E-01

oxidoreductase activity, acting on NADH or NADPH	3	4.30E-01	9.60E-01
electron carrier activity	5	5.40E-01	9.80E-01
Annotation Cluster 37: Enrichment Score: 1.82	Count	P_Value	Benjamini
Heat shock protein 70	3	1.30E-02	1.90E-01
Heat shock protein Hsp70	3	1.30E-02	1.90E-01
PIRSF002581:chaperone HSP70	3	1.30E-02	2.20E-01
Heat shock protein 70, conserved site	3	1.90E-02	2.60E-01
Antigen processing and presentation	7	2.00E-02	2.10E-01
Annotation Cluster 38: Enrichment Score: 1.75	Count	P_Value	Benjamini
ATP-grasp fold, subdomain 2	4	1.80E-03	4.00E-02
ligase	11	5.70E-03	3.20E-02
ligase activity, forming carbon-nitrogen bonds	5	5.80E-01	9.90E-01
Annotation Cluster 39: Enrichment Score: 1.65	Count	P_Value	Benjamini
multifunctional enzyme	6	2.00E-03	1.30E-02
purine biosynthesis	3	9.70E-03	4.80E-02
ligase activity, forming carbon-nitrogen bonds	5	5.80E-01	9.90E-01
Annotation Cluster 40: Enrichment Score: 1.59	Count	P_Value	Benjamini
MLL5-L complex	3	7.30E-03	6.30E-02
methyltransferase complex	3	4.80E-02	2.30E-01
histone methyltransferase complex	3	4.80E-02	2.30E-01
Annotation Cluster 41: Enrichment Score: 1.58	Count	P_Value	Benjamini
organelle localization	7	5.00E-03	9.20E-02
establishment of organelle localization	6	6.60E-03	1.10E-01
establishment of vesicle localization	3	1.10E-01	6.10E-01
vesicle localization	3	1.30E-01	6.60E-01
Annotation Cluster 42: Enrichment Score: 1.51	Count	P_Value	Benjamini
actin capping	4	1.70E-03	1.10E-02
cell cortex part	7	2.70E-03	2.80E-02
actin filament capping	4	6.00E-03	1.00E-01
negative regulation of actin filament depolymerization	4	7.70E-03	1.20E-01
cortical cytoskeleton	5	9.00E-03	7.50E-02
spectrin	3	9.30E-03	7.30E-02
repeat:Spectrin 10	3	9.80E-03	2.20E-01
repeat:Spectrin 11	3	9.80E-03	2.20E-01
repeat:Spectrin 12	3	9.80E-03	2.20E-01
repeat:Spectrin 13	3	9.80E-03	2.20E-01

repeat:Spectrin 14	3	9.80E-03	2.20E-01
repeat:Spectrin 15	3	9.80E-03	2.20E-01
repeat:Spectrin 16	3	9.80E-03	2.20E-01
repeat:Spectrin 17	3	9.80E-03	2.20E-01
regulation of actin filament depolymerization	4	1.10E-02	1.60E-01
repeat:Spectrin 7	3	1.20E-02	2.50E-01
repeat:Spectrin 6	3	1.20E-02	2.50E-01
repeat:Spectrin 9	3	1.20E-02	2.50E-01
repeat:Spectrin 8	3	1.20E-02	2.50E-01
negative regulation of actin filament polymerization	4	1.20E-02	1.70E-01
negative regulation of protein polymerization	4	1.30E-02	1.70E-01
negative regulation of organelle organization	6	1.30E-02	1.70E-01
repeat:Spectrin 5	3	1.30E-02	2.70E-01
actin cytoskeleton	11	1.50E-02	1.10E-01
negative regulation of protein complex assembly	4	2.00E-02	2.30E-01
repeat:Spectrin 4	3	2.90E-02	4.50E-01
repeat:Spectrin 3	3	3.20E-02	4.70E-01
negative regulation of protein complex disassembly	4	3.30E-02	3.20E-01
Spectrin repeat	3	3.70E-02	4.10E-01
repeat:Spectrin 1	3	4.30E-02	5.50E-01
repeat:Spectrin 2	3	4.30E-02	5.50E-01
SPEC	3	4.80E-02	4.00E-01
regulation of protein complex disassembly	4	5.70E-02	4.40E-01
regulation of actin filament polymerization	4	6.50E-02	4.80E-01
negative regulation of cytoskeleton organization	4	6.80E-02	4.90E-01
regulation of protein complex assembly	5	6.90E-02	4.90E-01
Spectrin/alpha-actinin	3	7.40E-02	6.10E-01
cortical actin cytoskeleton	3	7.90E-02	3.40E-01
regulation of organelle organization	8	8.00E-02	5.30E-01
regulation of cytoskeleton organization	6	8.50E-02	5.50E-01
regulation of actin polymerization or depolymerization	4	8.70E-02	5.50E-01
regulation of actin filament length	4	9.40E-02	5.70E-01
actin-binding	7	9.50E-02	3.10E-01
negative regulation of cellular component organization	6	9.80E-02	5.80E-01
regulation of protein polymerization	4	1.10E-01	6.20E-01
regulation of actin cytoskeleton organization	4	2.00E-01	7.80E-01
regulation of actin filament-based process	4	2.10E-01	8.00E-01
actin binding	9	2.10E-01	8.30E-01
regulation of cellular component biogenesis	5	2.30E-01	8.20E-01
regulation of cellular component size	7	3.20E-01	9.00E-01
cytoskeletal protein binding	11	3.90E-01	9.50E-01

Tight junction	4	6.80E-01	9.50E-01
Annotation Cluster 43: Enrichment Score: 1.47	Count	P_Value	Benjamini
identical protein binding	25	3.50E-04	7.40E-03
protein homodimerization activity	9	2.30E-01	8.50E-01
protein dimerization activity	11	4.80E-01	9.70E-01
Annotation Cluster 44: Enrichment Score: 1.45	Count	P_Value	Benjamini
Heat shock protein Hsp90, conserved site	3	2.00E-03	4.50E-02
PIRSF002583:heat shock protein, HSP90/HTPG types	3	9.90E-03	1.90E-01
Heat shock protein Hsp90	3	1.30E-02	1.90E-01
HATPase_c	3	4.50E-02	4.30E-01
ATP-binding region, ATPase-like	3	7.00E-02	5.90E-01
Prostate cancer	5	2.00E-01	6.70E-01
NOD-like receptor signaling pathway	3	4.80E-01	8.80E-01
Annotation Cluster 45: Enrichment Score: 1.43	Count	P_Value	Benjamini
magnesium	14	4.40E-03	2.60E-02
metal ion-binding site:Magnesium	6	1.70E-02	3.10E-01
magnesium ion binding	15	2.80E-02	2.80E-01
metal-binding	32	9.00E-01	1.00E+00
Annotation Cluster 46: Enrichment Score: 1.41	Count	P_Value	Benjamini
multifunctional enzyme	6	2.00E-03	1.30E-02
ribonucleotide metabolic process	8	1.30E-02	1.70E-01
ribonucleotide biosynthetic process	7	2.00E-02	2.30E-01
nucleobase biosynthetic process	3	2.30E-02	2.60E-01
ribonucleoside monophosphate biosynthetic process	3	5.90E-02	4.50E-01
nucleobase metabolic process	3	5.90E-02	4.50E-01
ribonucleoside monophosphate metabolic process	3	6.80E-02	4.90E-01
nucleoside monophosphate biosynthetic process	3	2.10E-01	8.00E-01
nucleoside monophosphate metabolic process	3	3.10E-01	8.90E-01
Annotation Cluster 47: Enrichment Score: 1.39	Count	P_Value	Benjamini
domain:KH 3	3	1.30E-02	2.70E-01
domain:KH 1	3	3.40E-02	4.90E-01
domain:KH 2	3	3.40E-02	4.90E-01
K Homology, type 1	3	8.20E-02	6.30E-01
K Homology, type 1, subgroup	3	9.10E-02	6.70E-01
Annotation Cluster 48: Enrichment Score: 1.31	Count	P_Value	Benjamini
26S proteasome subunit P45	3	4.20E-03	8.10E-02

Posttranslational modification, protein turnover, chaperones	8	4.30E-03	7.50E-02
negative regulation of ubiquitin-protein ligase activity during mitotic cell cycle	6	5.10E-03	9.20E-02
anaphase-promoting complex-dependent proteasomal ubiquitin-dependent protein catabolic process	6	5.10E-03	9.20E-02
proteasome	5	5.50E-03	3.10E-02
negative regulation of ubiquitin-protein ligase activity	6	5.80E-03	9.90E-02
negative regulation of ligase activity	6	5.80E-03	9.90E-02
regulation of ubiquitin-protein ligase activity during mitotic cell cycle	6	7.40E-03	1.20E-01
proteasomal protein catabolic process	7	8.20E-03	1.20E-01
proteasomal ubiquitin-dependent protein catabolic process	7	8.20E-03	1.20E-01
negative regulation of protein ubiquitination	6	8.80E-03	1.30E-01
regulation of ubiquitin-protein ligase activity	6	1.10E-02	1.60E-01
negative regulation of cellular protein metabolic process	9	1.30E-02	1.70E-01
regulation of ligase activity	6	1.30E-02	1.70E-01
ATPase, AAA-type, conserved site	4	1.30E-02	1.90E-01
negative regulation of protein metabolic process	9	1.50E-02	1.90E-01
negative regulation of protein modification process	7	1.70E-02	2.00E-01
proteasome complex	5	1.90E-02	1.30E-01
regulation of protein ubiquitination	6	2.90E-02	3.00E-01
positive regulation of ubiquitin-protein ligase activity during mitotic cell cycle	5	2.90E-02	3.00E-01
positive regulation of ubiquitin-protein ligase activity	5	3.20E-02	3.20E-01
Proteasome	5	3.30E-02	2.70E-01
regulation of cellular protein metabolic process	15	3.50E-02	3.40E-01
positive regulation of ligase activity	5	3.70E-02	3.50E-01
positive regulation of protein ubiquitination	5	5.60E-02	4.40E-01
macromolecule catabolic process	20	7.90E-02	5.30E-01
ubiquitin-dependent protein catabolic process	8	1.20E-01	6.50E-01
cellular macromolecule catabolic process	17	1.80E-01	7.60E-01
positive regulation of catalytic activity	13	1.80E-01	7.60E-01
negative regulation of molecular function	9	2.20E-01	8.00E-01
regulation of protein modification process	8	2.40E-01	8.30E-01
positive regulation of molecular function	13	3.10E-01	8.90E-01
negative regulation of catalytic activity	7	3.40E-01	9.10E-01
positive regulation of cellular protein metabolic process	6	3.70E-01	9.20E-01
modification-dependent protein catabolic process	12	4.00E-01	9.40E-01
modification-dependent macromolecule catabolic process	12	4.00E-01	9.40E-01

positive regulation of protein modification process	5	4.00E-01	9.40E-01
positive regulation of protein metabolic process	6	4.00E-01	9.40E-01
proteolysis involved in cellular protein catabolic process	12	4.60E-01	9.60E-01
cellular protein catabolic process	12	4.60E-01	9.60E-01
protein catabolic process	12	5.00E-01	9.70E-01
proteolysis	17	7.30E-01	1.00E+00
positive regulation of macromolecule metabolic process	8	9.90E-01	1.00E+00

Annotation Cluster 49: Enrichment Score: 1.3	Count	P_Value	Benjamini
domain:Actin-binding	3	2.70E-02	4.30E-01
Actinin-type, actin-binding, conserved site	3	4.30E-02	4.60E-01
CH	4	4.50E-02	4.80E-01
domain:CH 1	3	4.60E-02	5.70E-01
domain:CH 2	3	4.60E-02	5.70E-01
Calponin-like actin-binding	4	8.10E-02	6.40E-01
actin-binding	7	9.50E-02	3.10E-01

Annotation Cluster 50: Enrichment Score: 1.29	Count	P_Value	Benjamini
pyridoxal phosphate	5	7.90E-03	4.20E-02
vitamin B6 binding	4	6.80E-02	5.00E-01
pyridoxal phosphate binding	4	6.80E-02	5.00E-01
vitamin binding	5	1.90E-01	8.10E-01

Annotation Cluster 51: Enrichment Score: 1.27	Count	P_Value	Benjamini
cellular amino acid biosynthetic process	5	1.10E-02	1.60E-01
amino-acid biosynthesis	3	3.70E-02	1.40E-01
amine biosynthetic process	5	5.00E-02	4.20E-01
glutamine family amino acid metabolic process	4	6.00E-02	4.50E-01
aspartate family amino acid metabolic process	3	6.30E-02	4.70E-01
carboxylic acid biosynthetic process	6	1.30E-01	6.60E-01
organic acid biosynthetic process	6	1.30E-01	6.60E-01

Annotation Cluster 52: Enrichment Score: 1.27	Count	P_Value	Benjamini
purine nucleotide metabolic process	10	4.80E-03	9.00E-02
ribonucleotide metabolic process	8	1.30E-02	1.70E-01
purine nucleotide catabolic process	4	1.90E-02	2.20E-01
ATP catabolic process	3	3.00E-02	3.10E-01
purine ribonucleotide metabolic process	7	3.20E-02	3.20E-01
purine ribonucleoside triphosphate catabolic process	3	4.10E-02	3.80E-01
ribonucleoside triphosphate catabolic process	3	4.10E-02	3.80E-01
heterocycle catabolic process	5	4.30E-02	3.90E-01

purine nucleoside triphosphate catabolic process	3	5.00E-02	4.20E-01
nucleotide catabolic process	4	5.70E-02	4.40E-01
purine ribonucleotide catabolic process	3	5.90E-02	4.50E-01
nucleoside triphosphate catabolic process	3	6.30E-02	4.70E-01
ribonucleotide catabolic process	3	6.80E-02	4.90E-01
nucleobase, nucleoside and nucleotide catabolic process	4	7.70E-02	5.30E-01
nucleobase, nucleoside, nucleotide and nucleic acid catabolic process	4	7.70E-02	5.30E-01
ATP metabolic process	5	1.10E-01	6.00E-01
nitrogen compound catabolic process	4	1.10E-01	6.10E-01
purine ribonucleoside triphosphate metabolic process	5	1.40E-01	6.90E-01
ribonucleoside triphosphate metabolic process	5	1.40E-01	6.90E-01
purine nucleoside triphosphate metabolic process	5	1.60E-01	7.20E-01
nucleoside triphosphate metabolic process	5	1.90E-01	7.70E-01
Annotation Cluster 53: Enrichment Score: 1.26	Count	P_Value	Benjamini
nadp	7	1.50E-02	6.70E-02
binding site:NADP	3	4.90E-02	5.90E-01
nucleotide phosphate-binding region:NADP	3	2.30E-01	9.80E-01
Annotation Cluster 54: Enrichment Score: 1.26	Count	P_Value	Benjamini
Actin, conserved site	3	2.20E-02	2.80E-01
PIRSF002337:Actin	3	5.50E-02	6.10E-01
ACTIN	3	7.20E-02	4.50E-01
Actin/actin-like	3	1.10E-01	7.20E-01
Annotation Cluster 55: Enrichment Score: 1.17	Count	P_Value	Benjamini
repeat:HEAT 1	4	3.80E-02	5.20E-01
repeat:HEAT 2	4	3.80E-02	5.20E-01
repeat:HEAT 4	3	1.00E-01	8.40E-01
repeat:HEAT 3	3	1.30E-01	9.00E-01
Annotation Cluster 56: Enrichment Score: 1.12	Count	P_Value	Benjamini
regulation of cell cycle	13	1.20E-02	1.60E-01
regulation of cell cycle process	5	1.30E-01	6.60E-01
regulation of mitotic cell cycle	5	2.60E-01	8.50E-01
Annotation Cluster 57: Enrichment Score: 1.12	Count	P_Value	Benjamini
metal ion-binding site:Potassium	3	2.40E-03	7.60E-02
metal ion-binding site:Magnesium	6	1.70E-02	3.10E-01
potassium	4	2.20E-01	5.50E-01
potassium ion binding	4	3.90E-01	9.50E-01

alkali metal ion binding	4	7.70E-01	1.00E+00
Annotation Cluster 58: Enrichment Score: 1.05	Count	P_Value	Benjamini
short sequence motif:Prevents secretion from ER	7	1.00E-04	5.30E-03
Endoplasmic reticulum, targeting sequence	6	4.60E-04	1.50E-02
endoplasmic reticulum lumen	7	2.20E-03	2.60E-02
cellular homeostasis	12	1.80E-01	7.50E-01
endoplasmic reticulum part	9	2.30E-01	6.60E-01
endoplasmic reticulum	9	6.90E-01	9.60E-01
endoplasmic reticulum	12	9.30E-01	1.00E+00
disulfide bond	18	1.00E+00	1.00E+00
disulfide bond	15	1.00E+00	1.00E+00
signal	11	1.00E+00	1.00E+00
signal peptide	11	1.00E+00	1.00E+00
Annotation Cluster 59: Enrichment Score: 1.03	Count	P_Value	Benjamini
nitrogen compound biosynthetic process	16	4.90E-04	1.70E-02
nucleotide biosynthetic process	11	1.40E-03	3.60E-02
nucleobase, nucleoside, nucleotide and nucleic acid biosynthetic process	11	1.80E-03	4.40E-02
nucleobase, nucleoside and nucleotide biosynthetic process	11	1.80E-03	4.40E-02
purine nucleotide metabolic process	10	4.80E-03	9.00E-02
ribonucleotide metabolic process	8	1.30E-02	1.70E-01
purine nucleotide biosynthetic process	8	1.40E-02	1.70E-01
ribonucleotide biosynthetic process	7	2.00E-02	2.30E-01
purine ribonucleotide metabolic process	7	3.20E-02	3.20E-01
purine ribonucleotide biosynthetic process	6	5.10E-02	4.20E-01
ATP metabolic process	5	1.10E-01	6.00E-01
ATPase activity, coupled to transmembrane movement of substances	5	1.20E-01	7.00E-01
ATPase activity, coupled to movement of substances	5	1.30E-01	7.10E-01
hydrolase activity, acting on acid anhydrides, catalyzing transmembrane movement of substances	5	1.30E-01	7.00E-01
cation-transporting ATPase activity	3	1.30E-01	7.00E-01
ATPase activity, coupled to transmembrane movement of ions	4	1.40E-01	7.10E-01
purine ribonucleoside triphosphate metabolic process	5	1.40E-01	6.90E-01
ribonucleoside triphosphate metabolic process	5	1.40E-01	6.90E-01
purine nucleoside triphosphate metabolic process	5	1.60E-01	7.20E-01
primary active transmembrane transporter activity	5	1.70E-01	7.70E-01
P-P-bond-hydrolysis-driven transmembrane transporter activity	5	1.70E-01	7.70E-01
nucleoside triphosphate metabolic process	5	1.90E-01	7.70E-01

ATP biosynthetic process	4	2.00E-01	7.80E-01
purine ribonucleoside triphosphate biosynthetic process	4	2.40E-01	8.30E-01
ATPase activity, coupled to transmembrane movement of ions, phosphorylative mechanism	3	2.40E-01	8.50E-01
ribonucleoside triphosphate biosynthetic process	4	2.40E-01	8.30E-01
purine nucleoside triphosphate biosynthetic process	4	2.40E-01	8.30E-01
nucleoside triphosphate biosynthetic process	4	2.50E-01	8.40E-01
inorganic cation transmembrane transporter activity	4	4.90E-01	9.80E-01
monovalent inorganic cation transmembrane transporter activity	3	5.50E-01	9.80E-01
Alzheimer's disease	5	6.20E-01	9.20E-01
monovalent inorganic cation transport	3	9.70E-01	1.00E+00
ion transport	4	9.80E-01	1.00E+00
cation transport	5	9.90E-01	1.00E+00
metal ion transport	3	1.00E+00	1.00E+00
ion transport	5	1.00E+00	1.00E+00
Annotation Cluster 60: Enrichment Score: 1.01	Count	P_Value	Benjamini
Integrin Signaling Pathway	5	3.20E-02	8.70E-01
Erk1/Erk2 Mapk Signaling pathway	4	8.40E-02	8.00E-01
Signaling of Hepatocyte Growth Factor Receptor	3	3.50E-01	9.80E-01

Supplemental Table 3. The list of KEGG pathways obtained by DAVID software analysis based on the list of proteins shown in Supplemental Table 1: a partial list of proteins from HeLa cell forming corona on dopamine coated nanoparticles.

KEGG_PATHWAY Term	Count	p Value	Benjamini
hsa00020:Citrate cycle (TCA cycle)	15	0.000	0.000
hsa03030:DNA replication	14	0.000	0.000
hsa03040:Spliceosome	24	0.000	0.000
hsa05130:Pathogenic Escherichia coli infection	15	0.000	0.000
hsa03430:Mismatch repair	9	0.000	0.000
hsa00970:Aminoacyl-tRNA biosynthesis	11	0.000	0.000
hsa00010:Glycolysis / Gluconeogenesis	13	0.000	0.000
hsa00630:Glyoxylate and dicarboxylate metabolism	7	0.000	0.001
hsa00620:Pyruvate metabolism	10	0.000	0.002
hsa03050:Proteasome	9	0.002	0.025
hsa04540:Gap junction	12	0.004	0.048
hsa00640:Propanoate metabolism	7	0.004	0.047
hsa00280:Valine, leucine and isoleucine degradation	8	0.005	0.054
hsa03420:Nucleotide excision repair	8	0.005	0.054
hsa00270:Cysteine and methionine metabolism	7	0.005	0.055

hsa03410:Base excision repair	7	0.006	0.059

Supplemental Table 4. The list of Annotation Clusters obtained by DAVID software analysis based on the list of mRNAs found to be differentially expressed in nanoparticle treated cells. Two clusters with enrichment scores above 1 are presented.

Annotation cluster 1: Enrichment Score: 1.85	Count	P_Value	Benjamini
HLH	4	1.50E-04	1.50E-03
domain:Helix-loop-helix motif	4	2.50E-04	2.00E-02
Basic helix-loop-helix dimerisation region bHLH	4	3.30E-04	1.50E-02
71.Id_proteins_G0-to-S_cell_cycle	3	4.70E-04	2.30E-03
TGF-beta signaling pathway	4	9.50E-04	1.30E-02
negative regulation of molecular function	5	1.30E-03	3.20E-01
negative regulation of transcription factor activity	3	2.00E-03	2.50E-01
negative regulation of DNA binding	3	2.50E-03	2.20E-01
response to organic substance	6	3.40E-03	2.20E-01
negative regulation of binding	3	3.40E-03	1.80E-01
negative regulation of transcription from RNA polymerase II promoter	4	6.70E-03	2.20E-01
regulation of transcription factor activity	3	1.00E-02	2.80E-01
response to protein stimulus	3	1.10E-02	2.70E-01
regulation of DNA binding	3	1.40E-02	3.10E-01
negative regulation of transcription, DNA-dependent	4	1.50E-02	3.10E-01
negative regulation of RNA metabolic process	4	1.50E-02	3.00E-01
negative regulation of macromolecule metabolic process	5	2.10E-02	3.20E-01
regulation of binding	3	2.10E-02	3.10E-01
negative regulation of transcription	4	2.90E-02	3.80E-01
negative regulation of gene expression	4	3.70E-02	4.40E-01
negative regulation of nucleobase, nucleoside, nucleotide and nucleic acid metabolic process	4	3.80E-02	4.30E-01
negative regulation of nitrogen compound metabolic process	4	3.90E-02	4.30E-01
heart development	3	4.00E-02	4.20E-01
transcription repressor activity	3	4.40E-02	9.60E-01
negative regulation of macromolecule biosynthetic process	4	4.50E-02	4.40E-01
negative regulation of cellular biosynthetic process	4	4.80E-02	4.50E-01
negative regulation of biosynthetic process	4	5.00E-02	4.60E-01
developmental protein	4	5.10E-02	9.60E-01
transcription regulator activity	5	7.10E-02	9.30E-01
regulation of cell cycle	3	8.50E-02	6.10E-01
regulation of transcription from RNA polymerase II promoter	4	8.90E-02	5.90E-01
nucleus	8	1.70E-01	9.40E-01
regulation of transcription, DNA-dependent	5	2.60E-01	9.20E-01
regulation of RNA metabolic process	5	2.80E-01	9.20E-01

regulation of transcription	5	5.50E-01	1.00E+00
Annotation cluster 2: Enrichment Score: 1.16	Count	P_Value	Benjamini
apoptosis	4	5.70E-02	4.80E-01
programmed cell death	4	5.90E-02	4.80E-01
Apoptosis	3	6.40E-02	8.70E-01
cell death	4	8.70E-02	6.00E-01
death	4	8.80E-02	6.00E-01

Supplemental references

[1] T. Rajh, L. X. Chen, K. Lukas, T. Liu, M. C. Thurnauer, and D. M. Tiede, "Surface Restructuring of Nanoparticles: An Efficient Route for Ligand−Metal Oxide Crosstalk," The Journal of Physical Chemistry B, vol. 106, no. 41, pp. 10543-10552, 2002/10/01 2002.

[2] R. Bazak et al., "Cytotoxicity and DNA cleavage with core-shell nanocomposites functionalized by a KH domain DNA binding peptide," Nanoscale, vol. 5, no. 23, pp. 11394-9, Dec 7 2013.

[3] E. M. B. Brown et al., "Methods for assessing DNA hybridization of peptide nucleic acid-titanium dioxide nanoconjugates," (in English), Analytical Biochemistry, vol. 383, no. 2, pp. 226-235, Dec 15 2008.

[4] P. J. Endres, T. Paunesku, S. Vogt, T. J. Meade, and G. E. Woloschak, "DNA-TiO2 nanoconjugates labeled with magnetic resonance contrast agents," (in English), Journal of the American Chemical Society, vol. 129, no. 51, pp. 15760-+, Dec 26 2007.

[5] T. Paunesku et al., "Gadolinium-conjugated TiO2-DNA oligonucleotide nanoconjugates show prolonged intracellular retention period and T1-weighted contrast enhancement in magnetic resonance images," (in eng), Nanomedicine, vol. 4, no. 3, pp. 201-7, Sep 2008.

[6] T. Paunesku et al., "Biology of TiO2-oligonucleotide nanocomposites," (in eng), Nat Mater, vol. 2, no. 5, pp. 343-6, May 2003.

[7] T. Paunesku et al., "Intracellular distribution of TiO2-DNA oligonucleotide nanoconjugates directed to nucleolus and mitochondria indicates sequence specificity," (in eng), Nano Lett, vol. 7, no. 3, pp. 596-601, Mar 2007.

[8] K. T. Thurn et al., "Endocytosis of titanium dioxide nanoparticles in prostate cancer PC-3M cells," Nanomedicine, vol. 7, no. 2, pp. 123-30, Apr 2011.

[9] K. T. Thurn et al., "Labeling TiO2 nanoparticles with dyes for optical fluorescence microscopy and determination of TiO2-DNA nanoconjugate stability," (in eng), Small, vol. 5, no. 11, pp. 1318-25, Jun 2009.

[10] A. G. Wu et al., "Titanium dioxide nanoparticles assembled by DNA molecules hybridization and loading of DNA interacting proteins," (in English), Nano, vol. 3, no. 1, pp. 27-36, Feb 2008.

[11] Y. Yuan et al., "Epidermal growth factor receptor targeted nuclear delivery and high-resolution whole cell X-ray imaging of Fe3O4@TiO2 nanoparticles in cancer cells," (in eng), ACS Nano, vol. 7, no. 12, pp. 10502-17, Dec 23 2013.

[12] H. C. Arora et al., "Nanocarriers enhance Doxorubicin uptake in drug-resistant ovarian cancer cells," (in eng), Cancer Res, vol. 72, no. 3, pp. 769-78, Feb 01 2012.

[13] A. Michelmore, W. Q. Gong, P. Jenkins, and J. Ralston, "The interaction of linear polyphosphates with titanium dioxide surfaces," (in English), Physical Chemistry Chemical Physics, Article vol. 2, no. 13, pp. 2985-2992, 2000.